



**Sudan University of Science & Technology**

**College Graduate Studies**



**Effect of Doping Carbon Nanotubes with Magnesium Oxide on its  
Structural and Optical Properties and Used in Diode Multilayers**

**أثر تشويب أنابيب الكربون النانوية بأوكسيد الماغنيسيوم على خصائصها التركيبية  
والضوئية واستخدامها كثنائي متعدد الطبقات**

A thesis submitted for Fulfillment Requirement of the Degree of  
Doctor of Philosophy in Physics

By:

**Maysa Elkheir Ali Sheik Edreis**

Supervisor by:

Prof.Dr. Khalid Mohammed Haroun

Co-Supervisor by:

Dr. Ahmed Elhassan Alfaki

**March 2022**

الايه

بسم الله الرحمن الرحيم

قال تعالى:

{ يَرْفَعُ اللَّهُ الَّذِينَ آمَنُوا مِنْكُمْ وَالَّذِينَ أُوتُوا الْعِلْمَ دَرَجَاتٍ وَاللَّهُ بِمَا تَعْمَلُونَ خَبِيرٌ }

(صدق الله العظيم)

[المجادله 11 ]

# Dedication

*I dedicate to my dear mother, starlit  
dear father I am Convicted you for all  
this , all my brothers , Sisters and my  
colleagues comrades the trail ,Thanks  
to all of them for help me enable  
complete my research I dedicated this  
research, , and all those who love me  
honestly, and I love them equally.*

## **Acknowledgements**

*First of all I should offer my thanks obedience and gratitude to Allah . most gracious merciful from whom I receive guidance and help .*

*and especially thank to supervisor of this research Prof.Dr. Khalid Mohammed Haroun and co-supervisor Dr. Ahmed Elhassan Alfaki, represented to in section of physics , And especially thank also for each of the financially or cognitively contributed to the completion of this research modest*

## Abstract

Carbon nanotube is long thin cylinders of graphite, it is made up of layers of carbon atoms every atom is connected evenly to three carbons arranged in a hexagonal lattice. In this research carbon nanotubes (CNTs) doping by magnesium oxide in different ratio (0.1, 0.3, 0.5, 0.7 and 0.9) from soot and coal, were synthesized using thermal chemical vapour deposition (CVD), and used in diode Multilayers fabrication. Five samples of CNTs prepared from each source were doped by magnesium oxide in different ratio (0.1, 0.3, 0.5, 0.7 and 0.9). X-ray diffraction technique (XRD) was used to obtain crystal structure and lattice parameters of samples, UV-Visible used to evaluate the optical properties. Fourier Transform Infrared spectroscopy (FTIR) used to measure the vibrational frequencies of bonds in the molecules.

XRD results showed that the increasing in concentration of magnesium oxide leads to change structure parameter of carbon nanotubes samples (grain size, d-space, density and miller indices) FTIR showed different vibrational frequencies for CNTs from soot and coal, also showed that CNTs from coal more stable than CNTs from soot. For the optical properties the absorbance of CNTs from soot greater than CNTs from coal, for Soot samples the decrease of absorption at wavelengths 317 nm corresponding photon energy 3.912 eV by MgO concentration increase, and for Coal samples decrease at wavelengths 272 nm corresponding photon energy 4.559 eV by MgO concentration increase. The optical energy band gap decrease with MgO concentration increase, the optical band gap for soot and coal of CNTS within range of semiconductor materials (3.392-3.517) eV. Finally, the I-V Curve display that the samples are diode multilayer the charge injection voltage and turn off voltage increases when the concentration of MgO and number of layer increases for CNTS made from soot and coal. These results confirm the previous studies.

## المستخلص

الأنابيب النانوية الكربونية عبارة عن أسطوانات رفيعة طويلة من الجرافيت ، تتكون من طبقات من ذرات الكربون كل ذرة متصلة بشكل متساو بثلاثة ذرات كربون مرتبة في شبكة سداسية الشكل . في هذا البحث تم تصنيع الأنابيب النانوية الكربونية (CNTs) وتشويهاها بواسطة أكسيد المغنيسيوم بتركيز مختلفة (0.1 ، 0.3 ، 0.5 ، 0.7 و 0.9) من مصدري السناج والفحم باستخدام طريقة الترسيب بالبخار الكيميائي الحراري (CVD) واستخدامها لتصنيع الصمام الثنائي متعدد الطبقات. تم تحضير خمس عينات من الأنابيب النانوية الكربونية من كل مصدر وتشويهاها بواسطة أكسيد المغنيسيوم بتركيز مختلفة (0.1 ، 0.3 ، 0.5 ، 0.7 و 0.9). استخدمت تقنية حيود الأشعة السينية (XRD) للحصول على البنية البلورية ومعاملات الشبكة البلورية للعينات ، كما تم استخدام مطيافية فورييه لتحويل الأشعة تحت الحمراء (FTIR) لقياس الترددات الاهتزازية للروابط في الجزيء. استخدمت الأشعة فوق البنفسجية المرئية لدراسة الخصائص البصرية.

أوضحت نتائج XRD ان الزيادة في تركيز اكسيد المغنيسيوم تؤدي إلى تغيير البنية التركيبية لعينات الأنابيب النانوية الكربونية (حجم الحبيبات ، المسافة بين المستويات الذرية، الكثافة ومعاملات ميلر )، كما أدى ذلك الى تغيير نوع خلية الوحدة الاساسية لجميع العينات. اظهرت مطيافية فورييه لتحويل الأشعة تحت الحمراء ترددات اهتزازية مختلفة للأنابيب النانوية الكربونية من الفحم والسناج ، كما أظهر أن انابيب النانوية الكربونية من الفحم أكثر استقراراً من انابيب النانوية الكربونية من السناج. بالنسبة للخصائص الضوئية ، فإن امتصاص الأنابيب النانوية الكربونية من السناج أكبر من الأنابيب النانوية الكربونية من الفحم، ينخفض الامتصاص عند الطوال الموجي 317 نانومتر بطاقة فوتون 3.912 إلكترون فولت بزيادة تركيز اكسيد المغنيسيوم بالنسبة لعينات السناج ، ولعينات الفحم ينخفض عند الطوال الموجي 272 نانومتر بطاقة فوتون 4.559 إلكترون فولت بزيادة تركيز اكسيد المغنيسيوم. تتناقص فجوة نطاق الطاقة الضوئية مع زيادة بزيادة تركيز اكسيد المغنيسيوم للفحم والسناج. فجوة النطاق الضوئية للأنابيب النانوية الكربونية من السناج والفحم ضمن نطاق مواد أشباه الموصلات (3.392-3.517) إلكترون فولت. أخيراً ، منحى الجهد والتيار للصمام الثنائي متعدد الطبقات ، يزداد جهد الحاجز و جهد التشبع بزيادة تركيز اكسيد المغنيسيوم وعدد الطبقات للأنابيب النانوية الكربونية المصنوع من السناج والفحم . هذه النتائج تتوافق مع الدراسات السابقة.

## List of Contents

Figure No.	Subject	Page No.
	استهلال	I
	Dedication	II
	Acknowledgements	III
	Abstract	I V
	المستخلص	V
	List of contents	VI
	List of Abbreviation	XI
	List of figures	XIII
	List of table	XVI
<b>Chapter one</b>		
1.1	carbon nanotube	1
1.2	Research Problem	2
1.3	Research objectives	2
1.3.1	General objective	2
1.3.2	Specific objectives	3
1.4	Research methodology	3
1.5	Layout of thesis	3
<b>Chapter two</b>		
2.1	Introduction	4
2.2	Carbon	4
2.3	Nano carbon Material	4
2.3.1	Fullerenes	4
2.3.2	Graphene	4
2.3.3	Nano diamond	5

2.4	Carbon Nanotubes	5
2.5	Classification of carbon nanotubes	6
2.5.1	Single-Walled Carbon Nanotube	6
2.5.2	Multi-Walled Carbon Nanotube	6
2.6	Synthesis methods for CNT	7
2.6.1	Laser ablation	7
2.6.2	Arc discharge	7
2.6.3	Chemical vapor deposition	8
2.6.3.1	Plasma Enhanced CVD (PECVD)	9
2.6.3.2	Thermal chemical vapor deposition	9
2.7	Properties of carbon nanotubes	10
2.7.1	Physical and chemical properties	10
2.7.2	Electrical	10
2.7.4	Thermal Properties	11
2.7.5	Optical Properties	12
2.8	X-ray Diffraction and Bragg's Law	12
2.9	Miller indices	13
2.10	Bravais Lattice	13
2.11	Type of Bravais Lattices	13
2.11.1	Cubic Systems	13
2.11.2	Orthorhombic Systems	13
2.11.3	Tetragonal Systems	13

2.11.4	Monoclinic Systems	14
2.11.5	Triclinic System	14
2.11.6	Rhombohedral System	14
2.11.7	Hexagonal System	14
2.12	Spectroscopy	15
2.13	Optical Properties	15
2.13.1	Absorption	15
2.13.2	Transmission	15
2.13.3	Absorption Coefficient	16
2.13.4	Extinction coefficient	16
2.13.5	Optical Energy Band gap	17
2.14	Semiconductor	17
2.15	Diode	17
2.15.1	Diode PN Junction Structure	17
2.15.2	PN junction diode in forward bias	18
2.15.3	PN junction diode in reverse bias	18
2.15.4	Types of diode	18
2.16	I-V Curve	19
2.17	Magnesium Oxide	20
2.18	Previous studies	21
2.18 .1	Comparison of electrical and optical behaviors of MEH-PPV and MEH-PPV/CNT blend based polymer light emitting diodes	21

2.18.2	Carbon Nanotubes -Reinforcing MgO-Doped Al <sub>2</sub> O <sub>3</sub> Nano composites	21
2.18.3	Synthesis and characterization studies of cadmium doped MgO Nano crystals for optoelectronics application	21
2.18.4	Magnesium Oxide (MgO) pH-sensitive Sensing Membrane in Electrolyte-Insulator-Semiconductor Structures with CF <sub>4</sub> Plasma Treatment	22
2.18.5	Effect of Nano-carbon percentage on properties of composite material	22
2.18.6	Synthesis and Characterization of Ce Doped MgO Nano crystals	23
2.18.7	Enhanced Structural, Thermal, and Electrical Properties of Multiwall Carbon Nanotubes Hybridized with Silver Nanoparticle	23
2.18.8	Synthesis and investigation of SiO <sub>2</sub> - MgO coated MWCNTs and their potential application	24
2.18.9	Graphene Oxide-Doped MgO Nanostructures for Highly Efficient Dye Degradation and Bactericidal Action	24
2.18.10	Doping Effect of CNT and Nano-Carbon in Magnesium Debride Bulk	24
2.18.11	Carbon Nanotubes (CNTs)-Reinforced Magnesium- Based Matrix Composites: A Comprehensive Review	25
2.18.12	Incorporating aligned carbon nanotube electrode arrays in organic thin-film transistors	26
2.18.13	Comparative Study of Deposit through a Membrane and Spin-Coated MWCNT as a Flexible Anode for Optoelectronic Applications	26
2.18.14	Charge Transfer Properties in MEH-	27

	PPV/PS:MWCNTs Nano composites	
2.18.15	High Luminance Organic Light-Emitting Diodes with Efficient Multi-Walled Carbon Nanotube Hole Injectors	27
2.18.16	Properties of Single-Walled Carbon Nanotube-Based Poly(phenylene vinylene) Electroluminescent Nano composites	27
<b>Chapter three</b>		
3.1	Introduction	29
3.2	Materials	29
3.3	Tools	29
3.4	Method	29
3.4.1	Preparation of MgO	29
3.4.2	Synthesizing carbon nanotube and doping by MgO	30
3.4.3	spin casting of Carbon Nano Tube (CNT) and MEH-PPV	30
3.5	Characterization Techniques	30
3.5.1	UV-Vis Spectroscopy	31
3.5.2	Fourier transforms infrared spectroscopy (FTIR)	31
3.5.3	X-ray diffraction (XRD)	32
3.5.4	I-V characteristics multilayers	33
<b>Chapter Four</b>		
4.1	Introduction	34
4.2.1	XRD Results of Carbon Nano Tube (CNT) doping by (Mg O)	34

4.2.2	XRD Discussion of Carbon Nano Tube (CNT) doping by (MgO)	41
4.3.1	FTIR Results of Carbon Nano Tube (CNT) doping by (MgO)	42
4.3.2	FTIR Discussion of Carbon Nano Tube (CNT) doping by (MgO)	46
4.4.1	Optical Results of Carbon Nano Tube (CNT) doping by (MgO)	46
4.4.2	Optical Discussion of Carbon Nano Tube (CNT) doping by (MgO)	49
4.5.1	I-V characteristics multilayers Results of Carbon Nano Tube (CNT) doping by (MgO)	51
4.5.2	I-V characteristics multilayers Discussion of Carbon Nano Tube (CNT) doping by (MgO)	59
4.5.3	General discussion	61
4.6	Conclusion	62
4.7	Recommendation	62
4.8	Referance	63

## List of Abbreviation

Abbreviations	Terminology
CNTS	Carbon Nanotube
MgO	Magnesium oxide
SWCNT	Single-Walled Carbon Nanotube
MWCNT	Multi-Walled Carbon Nanotube
CVD	Chemical vapor deposition
PECVD	Plasma Enhanced Chemical vapor deposition
XRD	X-ray diffraction
FTIR	Fourier Transform Infrared
MEH- PPV	Methoxy Ethylhexoxy Phenylene –Vinylene
UV	UV-Vis Spectroscopy
ITO	indium tin oxide
$E_g$	Energy gab band
PVD	Physical vapor deposition
SEM	Scanning electron microscopy
ISFET	Ion-sensitive field-transistor
TG	Thermo gravimetric
DTA	Differential thermal analysis
UVDRS	Uv diffused reflectance spectroscopy
AC	Arc discharge
LA	Laser ablation
OTFTs	Organic thin film transistors
PL	Photo luminescence
GNPs	Grapheme nano-platelets
NC	Nano carbon
GO	Graphene oxide
GNPs	Graphene nano platelets
PET	Poly ethylene terephthalate

## List of Figures

<b>Figures No.</b>	<b>Title</b>	<b>Page No.</b>
(2.1)	Single-Walled Carbon Nanotube (SWCNT), Multi-Walled Carbon Nanotube (MWCNT)	6
(2.2)	illustrates how diffraction of x-rays by crystal planes allows one to derive lattice spacing's by using the Bragg's law	12
(2.3)	The three possible types of cubic cells have been illustrated below	13
(2.4)	The four types of orthorhombic systems	13
(2.5)	The two types of tetragonal systems	14
(2.6)	The two possible types of monoclinic systems	14
(2.7)	Simple type of triclinic cell	14
(2.8)	Type of primitive rhombohedra cell	14
(2.9)	Simple type of hexagonal cells	15
(2.10)	PN junction diode in forward bias	19
(2.11)	I-V Curve of a Diode	20
(3.1)	spin casting of Carbon Nano Tube (CNT) and MEH-PPV	22
(3.2)	UV-Vis Spectroscopy	31
(3.3)	FTIR Spectroscopy	32
(3.4)	XRD	32
(3.5)	IV circuit	33
(4.1)	XRD spectrum of Carbon Nano Tube (CNT) from Soot and doping by Magnesium Oxide (MgO) <sub>0.1</sub> ratio	34
(4.2)	XRD spectrum of Carbon Nano Tube (CNT) from Soot and doping by Magnesium Oxide (MgO) <sub>0.3</sub> ratio	35
(4.3)	XRD spectrum of Carbon Nano Tube (CNT) from Soot and doping by Magnesium Oxide (MgO) <sub>0.5</sub> ratio	35
(4.4)	XRD spectrum of Carbon Nano Tube (CNT) from Soot and doping by Magnesium Oxide (MgO) <sub>0.7</sub> ratio	36
(4.5)	XRD spectrum of Carbon Nano Tube (CNT) from Soot and doping by	36

	Magnesium Oxide (MgO) 0.9 ratio	
(4.6)	XRD spectrum of Carbon Nano Tube (CNT) samples that made from Soot doping by Magnesium Oxide (MgO) (0.1, 0.3, 0.5, 0.7 and 0.9) ratio	37
(4.7)	XRD spectrum of Carbon Nano Tube (CNT) from Coal and doping by Magnesium Oxide (MgO) 0.1 ratio	38
(4.8)	XRD spectrum of Carbon Nano Tube (CNT) from Coal and doping by Magnesium Oxide (MgO) 0.3 ratio	38
(4.9)	XRD spectrum of Carbon Nano Tube (CNT) from Coal and doping by Magnesium Oxide (MgO) 0.5 ratio	39
(4.10)	XRD spectrum of Carbon Nano Tube (CNT) from Coal and doping by Magnesium Oxide (MgO) 0.7 ratio	39
(4.11)	XRD spectrum of Carbon Nano Tube (CNT) from Coal and doping by Magnesium Oxide (MgO) 0.9 ratio	40
(4.12)	XRD spectrum of Carbon Nano Tube (CNT) samples that made from Coal doping by Magnesium Oxide (MgO) (0.1, 0.3, 0.5, 0.7 and 0.9) ratio	40
(4.13)	IR spectrum of CNTs from (Soot) + Magnesium Oxide (MgO) (0.1, 0.3, 0.5, 0.7 and 0.9) Molar samples	43
(4.14)	IR spectrum of CNTs from (Coal) + Magnesium Oxide (MgO) (0.1, 0.3, 0.5, 0.7 and 0.9) s ratio amples	44
(4.15)	the relation between absorbance and wavelengths of (Soot and Coal) + Magnesium Oxide (MgO) (0.1, 0.3, 0.5, 0.7 and 0.9) ratio samples	47
(4.16)	Shows the relation between transmission and wavelengths for (Soot and Coal) +Magnesium Oxide (MgO) (0.1, 0.3, 0.5, 0.7 and 0.9) ratio samples.	47
(4.17)	the relation between absorption coefficient and wavelengths of (Soot and Coal) + Magnesium Oxide (MgO) (0.1, 0.3, 0.5, 0.7 and 0.9) ratio samples	48
(4.18)	the relation between extinction coefficient and wavelengths of (Soot and Coal)	48
(4.19)	the optical energy band gap of (Soot and Coal) + Magnesium Oxide (MgO) (0.1, 0.3, 0.5, 0.7 and 0.9) ratio samples	49
(4.20)	I-V characteristics of Soot Carbon Nano Tube (CNT) doping by Magnesium	51

	Oxide (MgO) 0.0	
(4.21)	I-V characteristics of Soot Carbon Nano Tube (CNT) doping by Magnesium Oxide (MgO) 0.1	52
(4.22)	I-V characteristics of Soot Carbon Nano Tube (CNT) doping by Magnesium Oxide (MgO) 0.3	52
(4.23)	I-V characteristics of Soot Carbon Nano Tube (CNT) doping by Magnesium Oxide (MgO) 0.5	53
(4.24)	I-V characteristics of Soot Carbon Nano Tube (CNT) doping by Magnesium Oxide (MgO) 0.7	53
(4.25)	I-V characteristics of Soot Carbon Nano Tube (CNT) doping by Magnesium Oxide (MgO) 0.9	54
(4.26)	I-V characteristics of Coal Carbon Nano Tube (CNT) doping by Magnesium Oxide (MgO) 0.0	54
(4.27)	I-V characteristics of Coal Carbon Nano Tube (CNT) doping by Magnesium Oxide (MgO) 0.1	55
(4.28)	I-V characteristics of Coal Carbon Nano Tube (CNT) doping by Magnesium Oxide (MgO) 0.3	55
(4.29)	I-V characteristics of Coal Carbon Nano Tube (CNT) doping by Magnesium Oxide (MgO) 0.5	56
(4.30)	I-V characteristics of Coal Carbon Nano Tube (CNT) doping by Magnesium Oxide (MgO) 0.7	56
(4.31)	I-V characteristics of Coal Carbon Nano Tube (CNT) doping by Magnesium Oxide (MgO) 0.9	57
(4.32)	relationship between concentration of Magnesium Oxide (MgO) and charge	58
	injection voltage for Carbon Nano Tube (CNT) from (Soot and Coal)	
(4.33)	relationship between concentration of Magnesium Oxide (MgO) and turn on Voltage for Carbon Nano Tube (CNT) from (Soot and Coal)	58

## List of Tables

<b>Table No.</b>	<b>Title</b>	<b>Page No.</b>
(4.1)	Calculate Lattice Constants from Peak Locations and Miller Indices of Carbon Nano Tube (CNT) samples that made from Soot doping by Magnesium Oxide (MgO) (0.1, 0.3, 0.5, 0.7 and 0.9) ratio	37
(4.2)	Calculate Lattice Constants from Peak Locations and Miller Indices of Carbon Nano Tube (CNT) samples that made from Coal doping by Magnesium Oxide (MgO) (0.1, 0.3, 0.5, 0.7 and 0.9) ratio	41
(4.3)	Characteristic IR of CNTs from (Soot) + Magnesium Oxide (MgO) (0.1, 0.3, 0.5, 0.7 and 0.9) ratio samples	43
(4.4)	Characteristic IR of CNTs from (Coal) + Magnesium Oxide (MgO) (0.1, 0.3, 0.5, 0.7 and 0.9) ratio samples	45
(4.5)	Threshold Of Charge Injection And Highly Twistable Device Had Shown A Turn On Voltage Of Carbon Nano Tube (CNT) From (Soot And Coal) And Doping By Magnesium Oxide (Mgo) In Different Ratio (0.1, 0.3, 0.5, 0.7 And 0.9)	57

# Chapter One

## Introduction

### 1.1 carbon nanotube

Carbon nanotubes are one of the most commonly mentioned building blocks of nanotechnology. With one hundred times the tensile strength of steel, thermal conductivity better than all but the purest diamond (Yusof, 2016) and electrical conductivity similar to copper, but with the ability to carry much higher currents (Simo, 1993), they seem to be a wonder material. CNTs have special physical, biological and chemical activities (Chen, 1999). They are utilized for various purposes like solar cell, purification systems, fuel cells, as separation membranes, filters, displays, clothes, sensors, biomedical industry, for hydrogen storage and as a super capacitor (Ma, 2008). Inorganic nanoparticles such as metal oxides, gold, and carbon-based nanomaterial have acquired growing heed through the last ten years as possible transporters for diagnostics and therapeutics of several cancers. Carbon nanotubes were 'discovered' in 1991 by Iijima (Sumio, 1991), and have since been the subject of much research. It is effectively long thin cylinders of graphite made up of layers of carbon atoms every atom is connected evenly to three carbons arranged in a hexagonal lattice (Kim, 2000). The layers themselves are not chemically bonded to each other but held together by weak forces called Van der Waal. Nanoparticles are classified into two main forms: Multi-walled CNTs (MWCNTs), with diameters between 10nm to 50nm and a single-walled CNTs (SWCNTs), with diameters between 0.6nm and 3nm. SWCNTs consist of a roll of graphene sheet used in forming a cylinder; while MWCNTs are made of multiple rolls of cylinder (Kong, 1998). There are many other types of nanotube, from various inorganic kinds, such as those made from boron nitride, to organic ones, such as those made from self-assembling cyclic peptides (protein

components) or from naturally-occurring heat shock proteins (extracted from bacteria that thrive in extreme environments). Through arc discharge, laser ablation, and Chemical Vapor Deposition (CVD) CNTs were synthesized in large amounts (Ravishankar, 2011). CVD was regarded as the most suitable and cheap technique for growing different types of CNTs under mild environment (Ahmad, 2016). CNTs have been produced by different sources of carbon, Hydrocarbon precursor is needed to produce CNTs using CVD method. Methane and acetylene are the commonly used hydrocarbon (Kaviyarasu, 2011). Carbon monoxide, soot and coal are other sources of carbon used to produce CNT (Haur, 2017). It is difficult to prepare uniform samples of filled nanotubes. The surface of CNT cannot attach to metal precursors due to its chemically 'inert' and hydrophobic nature (Anvari, 2017). Thus, it is necessary to modify its surface to establish efficient tube-matrix contacts. The wide distribution of diverse functional groups like hydroxyl, carboxyl, and carbonyl on the surface of CNT can offer active sites for metal ions to attach (Poonguzhali, 2017). Magnesium oxide (MgO) is usually considered as a potential high surface-area material of CNTs. Nano scale magnesium oxide has special physical and chemical activities due to its structure. A lot of new techniques that can be used to prepare Nano-sized MgO particles (Sufri, 2014). Nonetheless, there is need to examine the many parameters that influence their production qualities and yields. There are more areas to research on the synthesis of CNTs and it can open way for the production of value-added products like carbon nanotubes. It is urgently needed to look for an ecofriendly and effective way to handle the organic contaminants in wastewater. Thus, it is necessary to produce carbon nanotube magnesium oxide composite that is efficient. The production and characterization of CNTs and MgO composites is necessary. The actual areas of use for carbon nanotubes are currently very limited, It is predicted that the largest field of application in the future will be composite

materials, which do not require as high purity and as well-defined characteristics as with many electronics applications such as diodes.

## **1.2 Research Problem**

The developments in semiconductor nanotechnology lead to new materials having specific Properties, which can be considered for electronic applications such as diodes, transistors and solar cells. This materials used in this filed in our country it is not available, very difficult synthesis and high cost. We shall search about alternative local material it has low cost, easy treatment and available such as soot and coal which can be used to synthesis carbon nanotubes to that have novel thermal and mechanical properties which it can enhancement the performance of electronics component.

## **1.3 Research objectives**

### **1.3.1 General objective**

Determination Optical and Structural Properties of carbon nanotubes doping by magnesium oxide (MgO) from two sources coal and soot made by thermal Chemical Vapor Deposition (CVD) method and used in Multilayers diode.

### **1.3.2 Specific objectives**

- To synthesis carbon nanotubes doping by magnesium oxide (MgO) from two sources coal and soot by thermal Chemical Vapor Deposition (CVD)
- To determine the crystal structure and lattice parameters of carbon nanotube doping by Magnesium Oxide using X-ray diffraction (XRD) technique.
- To measure the vibrational frequencies of bonds, and Functional Group using Fourier transforms infrared spectroscopy (FTIR).

- To obtain the optical properties (absorbance, transmission, absorption coefficient, extinction coefficient and optical energy band gap) using UV-Visible Spectroscopy.
- To fabricate film multilayer by using spin coating technique.
- To find out the IV curve of diode multilayer.

#### **1.4 Research methodology**

Synthesizing carbon nanotube from coal and soot doping by magnesium oxide in different molar (0.1, 0.3, 0.5, 0.7 and 0.9) by thermal Chemical Vapor Deposition (CVD). X-Ray Diffraction (XRD) , Fourier Transform Infra-Red Spectroscopy (FT-IR) and UV-Visible spectrometer were used to determine crystal structure and lattice parameters respectively to specify chemical bonds within atoms and Functional Groups, to obtain optical properties and Finally, film multilayer study was fabricated by using spin coating technique to study I-V characteristics of prepared samples.

#### **1.5 Layout of thesis**

This research contain four chapter, chapter one introduction, while chapter two concerned the theoretical background and previous studies. Chapter three explains the materials and method, and chapter four explains the Results, Discussion and the recommendation.

# Chapter Two

## Theoretical Background

### 2.1 Introduction

This chapter content of theoretical background about carbon nanotubes in details, spectroscopy, diodes and previous studies.

### 2.2 Carbon

### 2.3 Nano carbon Material

Carbon is one of the essentialfoundational elements of all life (Krueger, 2010). Carbon sources are any natural or artificial production site of carbon and any chemical compounds composed of carbon, such as carbon dioxide and methane. For example, the burning of fossil fuels, animal respiration, are all sources of carbon (Kharisov, 2019). These sources are worldwide. Another increasingly prevalent source of carbon is Plastics, micro plastics in particular (Gadipelli, 2017). when plastic degrades it releases carbon into soils, water, and the atmosphere One of the most important sources of carbon is carbon from burning wood and plants to produce charcoal and soot(Dai, 2001).

#### 2.3.1 Fullerenes

Fullerene is a spherical carbon compound and is an allotrope of carbon such as diamond, graphite and carbon nanotubes(Kuhlbusch, 1996). Fullerenes of C<sub>60</sub>, C<sub>70</sub> and C<sub>84</sub> are well known. They are isolable carbon compounds in a sole molecular species. the 60 carbon atoms consist of 12 five-membered rings and 20 six-membered rings. The most specific feature of fullerene is that it is an excellent electron acceptor (Tandabany, 2009)

#### 2.3.2 Graphene

Graphene, which is one of the Nano carbon materials, consists of all six-membered rings with sp<sup>2</sup> (Delhaes, 2000). Since graphite is formed by combination of

graphene with van der Waals force. However, details of the properties were unclear until late years. The interesting properties of graphite are due in large measure to the strong semi metallic bonds between carbon atoms in plane layers and to the relatively weak binding between planes. Thus graphite has a low vapor pressure and approximately two-dimensional electrical and thermal conductivity(Zondlo, 2012). It is easily deformed in slip on the basal plane, but in polycrystalline form it is relatively strong at high temperature. Graphene has proved the particular characteristics of electronic, mechanical, and chemical properties. The most characteristic feature of graphene is its electrical property (Chand, 2017).

### **2.3.3 Nano diamond**

Diamond, an allotrope of carbon, has excellent hardness(Shenderova, 2012), coefficient of friction, thermal conductivity, insulation characteristics, and refractive index. Large and highly pure diamond is good for use as jewelry(Georgakilas, 2015). Furthermore, the major industrial application of diamond is for cutting and polishing tools, because it is the hardest of natural products. However, diamond is not workable enough because of its hardness(Vaijayanthimala, 2009)

## **2.4 Carbon Nanotubes**

Carbon nanotube is long thin cylinders of graphite, it is made up of layers of carbon atoms where every atom is connected evenly to three carbons arranged in a hexagonal lattice (Iijima, 1993). The layers themselves are not chemically bonded to each other but held together by weak forces called Van der Waals. Carbon nanotubes are one of the most commonly mentioned building blocks of nanotechnology (Ma, 2008). With one hundred times the tensile strength of steel, thermal conductivity better than all, but the purest diamond, and electrical

conductivity similar to copper, but with the ability to carry much higher currents (Ebbesen, 1992). nanotubes come in a variety of type: long, short, single-walled, multi-walled, and open, closed, with different types of spiral structure, etc. Each type has specific using and applications especially in thermal conductivity and nonlinear optics, it has distinctive properties like, mechanical and electrical properties (Harris, 1997) ,The optical properties are important to be measured and investigated accurately, is an optical material with a very wide optical transmission .There are many other types of nanotube, from various inorganic kinds, such as those made from boron nitride, to organic ones, such as those made from self-assembling cyclic peptides (protein components) or from naturally-occurring heat shock proteins (extracted from bacteria that thrive in extreme environments) (Kim , 2000).

## **2.5 Classification of carbon nanotubes**

Carbon nanotubes are classified into two main forms:

### **2.5.1 Single-Walled Carbon Nanotube**

Single-Walled Carbon Nanotube (SWCNT) consist of a roll of graphene sheet used in forming a cylinder with diameters between 0.6nm and 3nm (Ganesh, 2013),These have fabricated in diameters different diameters of SWCNTs determined by the range of temperature at which they synthesized and method. Increasing temperature results in larger-sized (wider) SWCNTs have incorporated (Lee, 1997). The structure of SWCNTs may vary and may either be zigzag, helical, armchair or chiral arrangement. The surface area of SWCNTs is also considerably higher, at 1300 m<sup>2</sup>/g , which makes it ideal for nano-robotics and future of medicine administering (Ijima ,1992).

## 2.5.2 Multi-Walled Carbon Nanotube

Made of multiple rolls of cylinder with diameters between 10nm to 50nm it is have high physical, mechanical, and electrical activities. MWCNTs are weakly bounded by Van der Waals interactions in a tree ring-like structure (Ganesh ,2013). The most extreme can be made up of up to several hundred concentric cylinders with a typical distance between the layers of rapheme of  $\sim 0.34$  nm Even if carbon nanotubes are generally categorized into these two groups, each group can consist of a complex mixture of tubes of varying length, diameter, crystalline structure, surface chemistry(Charlier, 1999).

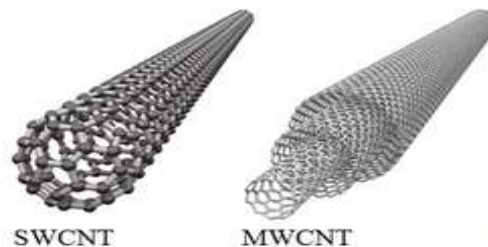


**Fig (2.1): Single-Walled Carbon Nanotube (SWCNT), Multi-Walled Carbon Nanotube (MWCNT) (Charlier, 1999).**

## 2.6 Synthesis methods for CNT

Generally, three techniques are being used for producing CNTs(Danikiewicz, 2013):

### 2.6.1 Laser ablation(LA)

LA it is a technique that using to production carbon nanotubes (Becker, 1997).The basic principle of LA is very simple and easy to perform. The specialty of this method is to use a laser source (Matsu, 2018).The setup consists of a reaction chamber in a quartz tube mounted in an adjustable hinged tube furnace/oven. Based on operator request, a target rod (either pure graphite for MWCNTs or metal graphite mixture for SWCNTs) is placed at middle high-temperature zone

(WanderWal, 2003). The quartz tube is then sealed at downstream end to pump. An inert gas or mixed gas composite is then entered the quartz tube at the upstream side of the tube. The pressure controller at downstream side is controlled to feed gas flow into the tube. A laser source like ND:YAG is then entered the quartz tube and is placed in such a way that it directly focuses onto the target rod at the middle. The laser power evaporated the target rod and produced many scattered carbon species. The inert gas or its composite flows sweep the carbon species to deposit them in a collector at the downstream of the tube. Before the inert gas escaped from the tube, it enters a water-cooled collector and filter to deposit CNTs (Ka, 2016).

### **2.6.2 Arc discharge(AC)**

It is a common and simple method to synthesize CNTs, and it was initially practiced for the synthesis of fullerenes. The method synthesizes CNTs with mixture of components like carbonaceous particles and metal catalysts, and hence, product purification is a must (Batani, 2014). In this method, a high current is applied through two graphite electrodes anode and cathode in a closed chamber. Plasma of inert gas is ignited at high temperature and low pressure into the chamber (Das, 2016). The two graphite electrodes are placed face to face with a gap. The applied current produces small carbon fragments by disrupting graphitic carbon networks in positive anode electrode. The fragments are then simultaneously deposited on the negative cathode electrode. Thus, the length of negative anode is decreased with the initiation of CNT production on the positive cathode electrode. Thus, the length and compositions of anode are directly proportional to the formation of CNTs on cathode electrode. The carbon nanotubes grow on the cathode while the anode is consumed (Mirabile, 2006). Carbon atoms are vaporized due to high temperature and pressure and released from anode graphite rod in the form of small carbon cluster subsequently, this cluster is

deposited on a precursor or metal surface catalyst on cathode electrode surface and rearranged them into microtubule-like CNT structure. However, the formation of desire CNTs (either SWCNTs or MWCNTs) largely depends on the inert gas, temperature, current, and catalysts used in the discharge chamber (Gattia, 2006) .

### **2.6.3 Chemical vapor deposition(CVD)**

Chemical vapor deposition(CVD) is a deposition process where chemical precursors are transported in the vapor phase to decompose on a heated substrate to form a film. The films may be epitaxial, polycrystalline or amorphous depending on the materials and reactor conditions(Yaceman, 1993).CVD has become the major method of film deposition for the semiconductor industry due to its high throughput, high purity, and low cost of operation. CVD is also commonly used in optoelectronics applications, optical coatings, and coatings of wear resistant parts(Vohts ,2006). CVD is based on the thermal decomposition of gaseous hydrocarbon in the presence of a metal catalyst such as iron, cobalt, nickel or yttrium. Gases containing carbon such as carbon dioxide,methane, and acetylene are led into an oven to be heated up. The heated gas reacts with the metal catalyst, which also acts as a “growth seeds”. Ethylene, benzene or xylene can also be used in the manufacturing process. With CVD, both MWCNT and SWCNT are produced, CVD has many advantages over physical vapor deposition (PVD) processes such as molecular beam evaporation and sputtering. Firstly, the pressures used in CVD allow coating of three dimensional structures with large aspect ratios. Since evaporation processes are very directional, PVD processes are typically line of sight depositions that may not give complete coverage due to shadowing from tall structures. Secondly, high precursor flow rates in CVD give deposition rates several times higher than PVD. Also, the CVD reactor is relatively simple and can be scaled to fit several substrates. Ultra-high vacuum is not needed for CVD and changes or additions of precursors is an easy task. Furthermore, varying

evaporation rates make stoichiometry hard to control in physical deposition. While for CVD stoichiometry is more easily controlled by monitoring flow rates of precursors (Hatton, 2008). Other advantages of CVD include growth of high purity films and the ability to fabricate abrupt junctions, The CVD method involves many of techniques:

### **2.6.3.1 Plasma Enhanced CVD (PECVD)**

A plasma is a partially ionized gas consisting of electrons and ions. Typical ionization fractions of  $10^{-5}$  to  $10^{-1}$  are encountered in process reactors. Plasmas are electrically conductive with the primary charge carriers being the electrons, The light mass of the electron allows it to respond much more quickly to changes in the field than the heavier ions. Most plasmas used for PECVD are generated using electric field. In the high frequency electric field, the light electrons are quickly accelerated by the field but do not increase the temperature of the plasma because of their low mass. The heavy ions cannot respond to the quick changes in direction and therefore their temperature stays low. Electron energies in the plasma have a Maxwellian distribution in the 0.1 – 20 eV range. These energies are sufficiently high to excite molecules or break chemical bonds in collisions between electrons and gas molecules. The high energy electrons in elastically collide with gas molecules resulting in excitation or ionization. The reactive species generated by the collisions do not have the energy barriers to reactions that the parent precursors do. Therefore, the reactive ions are able to form films at temperatures much lower than those required for thermal CVD (Varshney, 2014).

### **2.6.3.2 Thermal chemical vapor deposition**

There are two basic types of reactors for thermal CVD: the hot wall reactor and the cold wall reactor. a hot wall reactor is an isothermal furnace into which the substrates are placed. Hot wall reactors are typically very large and depositions are

done on several substrates at once. Since the whole chamber is heated, precise temperature control can be achieved with correct furnace design(kim, 2011). A disadvantage of the hot wall configuration is that deposition occurs on the walls of the chamber as well as on the substrate. As a consequence, hot wall reactors must be frequently cleaned to reduce flaking of particles from the walls which may contaminate the substrates. Furthermore, reactions in the heated gas and at the walls deplete the reactants and can result in feed rate limited growth.

In a cold wall reactor only the substrate is heated, usually by induction or radiant heating. Since most CVD reactions are endothermic, deposition is preferentially on the area of highest temperature. As a result, deposition is only on the substrate and the cooler reactor walls stay clean. Cold wall CVD has two main advantages over the hot wall configuration. First, particulate contamination is reduced since there are no deposits formed on the walls of the reactor. Second, since decomposition only occurs on the substrate there is no depletion of source gases due to reaction on the walls. However, hot wall reactors tend to have higher throughput since the designs more easily accommodate multiple wafer configurations(Tiwari, 2016) .

## **2.7 Properties of carbon nanotubes**

The strength of the carbon- bonds gives carbon nanotubes amazing properties(Ali ,2014). No previous material has displayed the combination of superlative properties such as;

### **2.7.1 Physical and chemical properties**

Carbon nanotubes are relatively stable and can be heated to above 500°C before they oxidize and burn up, Due to their structure, carbon nanotubes have a very high surface area compared to their mass. The ratio of surface area and mass of the tubes depends on their diameter and the degree to which they form bundles (Dresselhaus, 1998). Individual SWCNT have a ratio (area to mass) of about 1300

$m^2/g$  , while MWCNT typically have a ratio of around a few hundred  $m^2/g$  . Because SWCNT form themselves into bundles, the effective ratio of surface area and mass is often smaller or around  $\sim 300 m^2/g$  .The density of carbon nanotubes in powder form is very low and is dependent on the method of manufacture (Hussein , 2017).

### **2.7.2 Electrical**

Carbon nanotubes are both electrically conductive and semiconductors. The electrical characteristics of the tubes are primarily determined by their chiral angle, but for tubes with a small diameter also by their surface curvature. Theoretically, metallic carbon nanotubes can conduct electricity with a density that is 1,000 times greater than metals such as copper (Misewich, 2003). The electrical resistance of the tubes is determined by quantum mechanical phenomena and is independent of the tubes' length. There are many applications for the use of carbon nanotubes as electrical components. For example, diodes could be produced by merging SWCNT that have different electrical properties. It has also been shown that the electrical properties of the tubes change during deformation and stretching. This further increases the potential for the use of carbon nanotubes in electromechanical components such as sensors (Johannsen ,2016) .

### **2.7.3 Mechanical properties**

The strength of the carbon- bonds gives carbon nanotubes amazing mechanical properties one of the carbon nanotubes' coveted properties is that they have extreme strength. Single-walled carbon nanotubes are said to be around 10 times stronger than steel and 1-2 times stiffer (axial) than diamond and are considered to be one of the stiffest materials (ZH ,2007) , High mechanical (elasticity  $\sim 1$  TPa and tensile strength 50–500 GPa) Its excellent mechanical properties come from the strong covalent bonds ( $sp^2$  hybrids) that connect the carbon atoms in the rapheme

structure. Carbon nanotubes are not only strong, they are also elastic. You can press on the tip of a nanotube and cause it to bend without damaging to the nanotube, and the nanotube will return to its original shape when the force is removed. A nanotube's elasticity does have a limit (Goudal ,2013).

#### **2.7.4 Thermal Properties**

The strength of the atomic bonds in carbon nanotubes allows them to withstand high temperatures. Because of this, carbon nanotubes have been shown to be very good thermal conductors thermal stability ( $>700$  °C). When compared to copper wires, which are commonly used as thermal conductors, the carbon nanotubes can transmit over 15 times the amount of watts per meter per Kelvin(Wong,1997). The thermal conductivity of carbon nanotubes is depended on the temperature of the tubes and the outside environment Thermal Conductivity. The researches indicates that CNTs may be the best heat-conducting material man has ever known. Ultra-small SWNTs have even been shown to exhibit superconductivity (Hone ,2000)

#### **2.7.5 Optical Properties**

The optical properties of the carbon nanotubes indicate between light and matter (Chen , 2005). From an industrial standpoint, optical properties are of great importance, as they can contribute to determining the quality of the carbon nanotubes produced, by determining the carbon content, and in the detection of structural defects. The optical properties of carbon nanotubes are expected to be harnessed in the field of light-emitting diode and optical detectors (Singh ,2017).The peculiarities of these applications are not in their efficiency, as they are still weak, but rather in their selectivity for the emission and detection wavelengths, and in the possibility of improving them by means of the nanotube structure (Freitag , 2003).

## 2.8 X-ray Diffraction and Bragg's Law

X-ray diffraction (XRD) is a powerful nondestructive technique for characterizing crystalline materials, X-ray as a source to interact with carbon nanotubes gives details of characterization (Habeab, 2019).It can be reveal the local and global features of microstructure's lattice and crystalline phases, domain sizes, and impurities.It provides information on structures, phases, preferred crystal orientations (texture), and other structural parameters, such as average grain size, crystallinity, strain, and crystal defects.X-ray diffraction peaks are produced by constructive interference of a monochromatic beam of X-rays scattered at specific angles from each set of lattice planes in a sample(Dasa, 2015).The peak intensities are determined by the atomic positions within the lattice planes. Consequently, the X-ray diffraction pattern is the fingerprint of periodic atomic arrangements in a given material. An online search of a standard database for X-ray powder diffraction patterns enables quick phase identification for a large variety of crystalline samples considered Qualitative Analysis X-ray diffraction is the elastic scattering of x-ray photons by atoms in a periodic lattice. The scattered monochromatic X-ray that are in phase give constructive interference.X-ray techniques provide one of the non-destructive methods of measuring residual stresses. X-ray stress (strain) analysis is based on the Bragg diffraction equation (Zheng, 2004).

$$n\lambda = 2d\sin\theta \quad (2.1)$$

where  $n$  is an integer (diffraction order),  $\lambda$  the wavelength of the incident X-ray,  $d$  the interplanar spacing of the polycrystalline material under consideration, and  $\theta$  is the Bragg angle

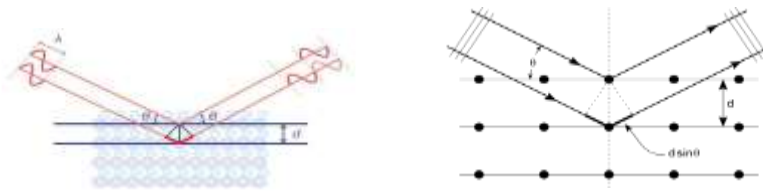


Figure (2.2) illustrates how diffraction of x-rays by crystal planes allows one to derive lattice spacings by using the Bragg's law (Zheng, 2004).

## 2.9 Miller indices

Used to specify directions and planes, the directions and planes could be in lattices or in crystals. This scheme advantage of eliminating all fractions from the notation for a plane. In the hexagonal system, which has four crystallographic axes, it is a group of three numbers that indicates the orientation of a plane or set of parallel planes of atoms in a crystal. If each atom in the crystal is represented by a point and these points are connected by lines, the resulting lattice may be divided into a number of identical blocks, or unit cells; the intersecting edges of one of the unit cells defines a set of crystallographic axes, and the Miller indices are determined by the intersection of the plane with these axes. The reciprocals of these intercepts are computed, and fractions are cleared to give the three Miller indices (hkl) (Hammond, 2015).

Top of Form

## 2.10 Bravais Lattice

There are several ways to describe a lattice. The most fundamental description is known as the Bravais lattice. In words, Bravais lattice is an array of discrete points with an arrangement and orientation that look exactly the same from any of the discrete points that is the lattice points are indistinguishable from one another. Thus Bravais lattice can refer to one of the of fourteen different types of unit cells that a crystal structure can be made up.

## 2.11 Type of Bravais Lattices

Out of fourteen types of Bravais lattices, seven types of Bravais lattices in three-dimensional, the letters a, b, and c have been used to denote the dimensions of the unit cells whereas the letters  $\alpha$ ,  $\beta$ , and  $\gamma$  denote the corresponding angles in the unit (Moeck, 2018).

### 2.11.1 Cubic Systems

In Bravais lattices with cubic systems, the following relationships can be observed

$$a = b = c \quad \alpha = \beta = \gamma = 90^\circ$$

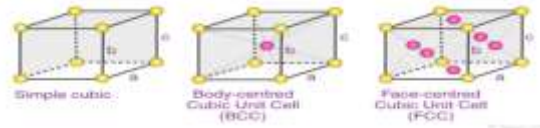


Figure (2.3) The three possible types of cubic cells have been illustrated (Li, 2015).

### 2.11.2 Orthorhombic Systems

The Bravais lattices with orthorhombic systems obey the following equations  $a \neq b$

$$\neq c \quad \alpha = \beta = \gamma = 90^\circ$$

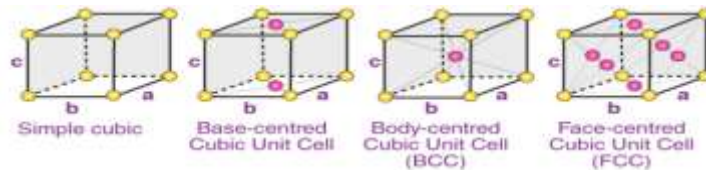


Figure (2.4) The four types of orthorhombic systems (Li, 2015).

### 2.11.3 Tetragonal Systems

In tetragonal Bravais lattices, the following relations are observed  $a = b \neq c$

$$\alpha = \beta = \gamma = 90^\circ$$

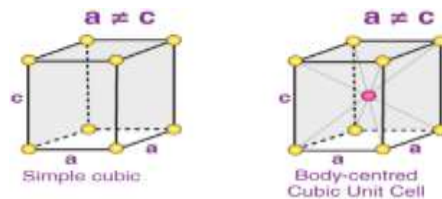


Figure (2.5) The two types of tetragonal systems(Li, 2015).

### 2.11.4 Monoclinic Systems

Bravais lattices having monoclinic systems obey the following relations:  $a \neq b \neq c$   
 $\beta = \gamma = 90^\circ$  and  $\alpha \neq 90^\circ$



Figure (2.6) The two possible types of monoclinic systems(Li, 2015).

### 2.11.5 Triclinic System

There exists only one type of triclinic Bravais lattice, which is a primitive cell. It obeys the following relationship  $a \neq b \neq c$  and  $\alpha \neq \beta \neq \gamma \neq 90^\circ$

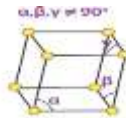


Figure (2.7) Simple type of triclinic cell(Li, 2015).

### 2.11.6 Rhombohedral System

Only the primitive unit cell for a rhombohedral system exists. Its cell relation is given by:  $a = b = c$  and  $\alpha = \beta = \gamma \neq 90^\circ$

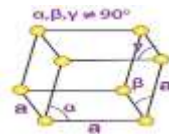


Figure (2.8) Type of primitive rhombohedral cell(Li, 2015).

### 2.11.7 Hexagonal System

The only type of hexagonal Bravais lattice is the simple hexagonal cell. It has the following relations between cell sides and angles  $a = b \neq c$  and  $\alpha = \beta = 90^\circ$  and  $\gamma = 120^\circ$  (Li, 2015).

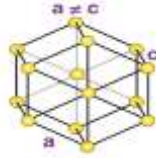


Figure (2.9) Simple type of hexagonal cell(Li, 2015).

## 2.12 UV-Vis Spectroscopy

It is the investigation and measurement of spectra produced by matter interacting with electromagnetic radiation. It is defined by the study of the interaction between matter and electromagnetic radiation. The electromagnetic spectrum comes from short and long wavelength  $10^{-4}$  nm to  $10^9$  nm. It is a field of analysis that uses the interaction of light to analyze and detect components within a sample. Light is shone and dispersed through the sample's compounds are excited by the electromagnetic radiation provided by a light source. Their molecules absorb energy from the electromagnetic radiation, become excited, and jump from a low energy ground state to a higher energy state of excitation. A detector, usually a photodiode, on the opposite side of the sample records the sample's absorption of wavelengths, and determines the extent of their absorption and creates a spectrum, which is unique to each compound of a different wavelength than the source's wavelength. Which can be used to determine the components, mass and luminosity of the sample (Donald, 2015).

## 2.13 Optical Properties

Optical methods are very useful for determining optical properties of material such as absorption, transmission, reflection and optical energy band gap (Heavens, 1991).

### 2.13.1 Absorption

When a light beam impinges on the surface of a material, part of the incident beam that is not reflected by the material is transmitted or absorbed through the material (Slavík, 1989).

$$I = I_0 \exp(-Bx) \quad (2.2)$$

where I=intensity of the beam coming out of the material I<sub>0</sub>= intensity of the incident beam x= path through which the photons move, and B= linear absorption coefficient.

### 2.13.2 Transmission

The phenomena transmission is the passing of electromagnetic radiation through a materil ,the material which have high value of absorption have small value of transmission and vies versa (dewit, 2013 ).

$$T = \frac{I}{I_0}$$

T = transmission,I<sub>0</sub>= intensity of the incident beam,I=intensity of the beam coming out of the material (2.3)

### 2.13.3 Absorption Coefficient

Different semiconductor materials have different absorption coefficients. Materials with higher absorption coefficients more readily absorb photons, which excite electrons into the conduction band. The absorption coefficient a measure of rate decreases in the intensity electromagnetic radiation when it pass through substance and much of the information about the properties of material obtain when the interact with electromagnetic radiation (Yosef, 2003).

Experimentally, the absorption coefficient ( $\alpha$ ) can be calculated from the relation:

$$\alpha = \frac{1}{t} \ln\left[\frac{(1-R)^2}{T}\right] \quad (2.4)$$

where t is the sample thickness, T and R are the transmission and reflection. But if you don't have T and R and you have Absorbance, then:

$$\alpha = 2.303 \frac{A}{t} \quad (2.5)$$

where  $\alpha$  is absorption coefficient , (A) is absorbance and (t) is thickness of thin film.

From Beer Lambert law

$$I = I_0 \exp(\alpha \times t) \quad (2.6)$$

thus,

$$\ln(I_0/I) = \alpha \times t$$

$$\alpha = (2.303 \times A) / t$$

where  $I_0$  = incident intensity,  $I$  = transmitted intensity,  $\alpha$  = absorption coefficient,  $t$  = Thickness of the material,  $A$  = absorbance

### 2.13.4 Extinction coefficient

Extinction coefficient measure of how strongly a substance absorb light at a particular wavelength. It is related to the absorption coefficient by (Andrew, 2004).

$$K = \frac{\alpha \lambda}{4\pi} \quad (2.7)$$

where  $\alpha$  is the absorption coefficient,  $k$  is the extinction coefficient, and  $\lambda$  is the wavelength in vacuum, where  $\lambda$  is the wavelength. If  $\lambda$  is in nm, multiply by  $10^7$  to get the absorption coefficient in the units of  $\text{cm}^{-1}$ .

### 2.13.5 Optical Energy Band gap

Band gap, also called an energy gap, is an energy range in a solid where no electronic states can exist. The band gap generally refers to the energy difference (in electron volts) between the top of the valence band and the bottom of the conduction band in insulators and semiconductors. The optical energy gap ( $E_g$ ) has been calculated by the relation

$$(\alpha h\nu)^2 = C(h\nu - E_g) \quad (2.8)$$

where  $(C)$  is constant. By plotting  $(\alpha h\nu)^2$  vs photon energy  $(h\nu)$  ( Comfort, 2016 ).

### 2.14 Semiconductor

Using in the manufacture of various kinds of electronic devices, including diodes, transistors, and integrated circuits. The study of semiconductor materials began in

the early 19th century. The elemental semiconductors are those composed of single species of atoms, such as silicon (Si), germanium (Ge), and tin (Sn) in column IV and selenium (Se) and tellurium (Te). Such devices are found in wide application because of their compactness, reliability, power efficiency, and low cost. As discrete components, they are found in use in power devices, optical sensors, and light emitters, including solid-state lasers. They have a wide range of current- and voltage-handling capabilities and, more important, lend themselves to integration into complex but readily manufacturable microelectronic circuits, and will be in the foreseeable future, the key elements for the majority of electronic systems, serving communications, signal processing, computing, and control applications in both the consumer and industrial markets (Seeger, 2013).

## **2.15 Diode**

The diode is one of the most important basic components in integrated circuit (Chen, 2016) and is one of the most ubiquitous electronic components and made of semi-conductive materials such as silicon and germanium, it has been intensively studied over the past century (Semple, 2009).

### **2.15.1 Diode PN Junction Structure**

Diode is a device consisting of the junction of an n-type and p-type semiconductor material. The wire connected to the p-type material is called the anode and the lead connected to the n-type material is the cathode. In general, the cathode of a diode is marked by a solid line on the diode.

### **2.15.2 PN junction diode in forward bias**

The positive terminal of the battery is connected to the P side (anode) and the negative terminal of the battery is connected to the N side (cathode) of the diode, holes in the p-type region and electrons in the n-type region are pushed towards the junction and begin to neutralize the depletion region, reducing the

displayed. Positive potential applied to a p-type material repels holes, while a negative potential applied to an n-type material repels electrons. The change in voltage between the p side and the n side decreases or switches the signal. As the forward bias voltage increases, the depletion region eventually becomes thin enough that the electric field of the region cannot counteract the movement of the charge carrier across the p-n junction, reducing the electrical resistance as a result. Electrons crossing the p-n junction into a p-type material (or holes crossing into an n-type material) will propagate into the near neutral region. The amount of minority diffusion in the quasi-neutral regions determines the amount of current that may flow through the diode (safa, 2001).

### **2.15.3 PN junction diode in reverse bias**

The positive terminal of the battery is connected to the N side (cathode) and the negative terminal of the battery is connected to the P (anode) side of the diode. Therefore, very little current will flow for the diode to break down. The positive terminal of the battery is connected to the N side (cathode) and the negative terminal of the battery is connected to the P (anode) side of the diode, and the 'holes' in the p-type material are pulled away from the junction, leaving behind charged ions and causing an increase in the width of the area depletion; Similarly, since the n-type region is attached to the positive terminal, the electrons will also be pulled away from the junction, with the same effect. This increases the voltage barrier resulting in a high resistance to the flow of charge carriers, allowing a minimum electric current to cross the pn junction. An increase in the junction resistance p n causes the junction to act as an insulator (safa, 2001).

## 2.15.4 Types of diode

- **Zener diod:** It works as a normal diode in forward bias, but it differs from a regular diode in reverse bias as it is designed to have a breakdown voltage greater than that of a regular diode (Gupta, 2017).
- **Light diode:** The light radiates when it is delivered in the forward direction (Marais, 2008).
- **Photodiodes:** It is affected by light, the more light, the greater the current (Lischke, 2015) .
- **Varactor diode:** It is connected in the reverse direction and is called a capacitive diode, as the capacitance changes with the voltage applied to it (Liu, 2014) .
- **Schottky diode :** It is uses less volts, and its disadvantages are small current(Chen, 2011)

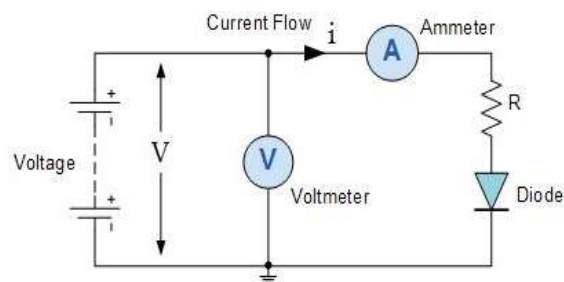


Figure (2.10) PN junction diode in forward bias( safa, 2001).

## 2.16 I-V Curve

The I-V Characteristic Curves, which is short for Current-Voltage Characteristic Curves or simply I-V curves of an electrical device or component, are a set of graphical curves which are used to define its operation within an electrical circuit. As its name suggests, I-V characteristic curves show the relationship between the current flowing through an electronic device and the applied voltage across its terminals. The relationship between voltage and current is linear and constant at a

constant temperature, such that current (I) is proportional to the potential difference V multiplied by the proportionality constant. However, practical resistors may exhibit nonlinear behavior under certain conditions, for example, when exposed to high temperatures. There are many electronic components and devices that have non-linear properties, that is, the  $V / I$  ratio is not constant like the diodes, transistors and solar cells. Semiconductor diodes have the characteristics of non-linear current and voltage as the current flowing through the forward-biased common silicon diode is limited by the resistance of the junction. When the diode is forward biased, anode positive with respect to the cathode, a forward or positive current passes through the diode and operates in the top right quadrant of its I-V characteristics curves as shown in figure (2.11). Starting at the zero intersection, the curve increases gradually into the forward quadrant but the forward current and voltage are extremely small. The current-voltage characteristics of an electronic component tells us much about its operation and can be a very useful tool in determining the operating characteristics of a particular device or component by showing its possible combinations of current and voltage, and as a graphical aid can help visually understand better what is happening within a circuit (LI, 2020 ).

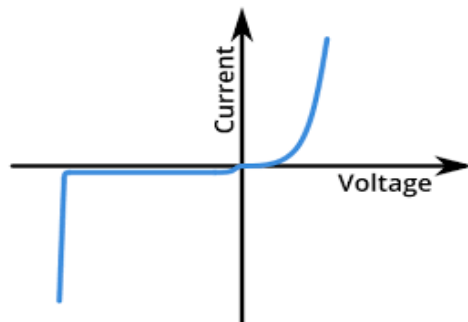


Figure (2.11) I-V Curve of a Diode (LI, 2020 ).

## **2.17 Magnesium Oxide**

Magnesium Oxide is a highly insoluble thermally stable Magnesium source suitable for glass, optic and ceramic applications. It is a hygroscopic white powder that forms magnesium hydroxide in the presence of water, historically known as magnesia alba (white mineral from Magnesia). Oxide compounds are not conductive to electricity. However, certain perovskite structured oxides are electronically conductive finding application in the cathode of solid oxide fuel cells and oxygen generation systems. They are compounds containing at least one oxygen anion and one metallic cation. They are typically insoluble in aqueous solutions (water) and extremely stable making them useful in ceramic structures as simple as producing clay bowls to advanced electronics and in light weight structural components in aerospace and electrochemical applications such as fuel cells in which they exhibit ionic conductivity. Metal oxide compounds are basic anhydrides and can therefore react with acids and with strong reducing agents in redox reactions. Magnesium Oxide is also available in different forms such as pellets, pieces, powder, sputtering targets, tablets, and nano powder. There are many methods to synthesize magnesium oxide nanoparticles like hydrothermal method chemical method sol-gel method combustion method and electro spinning method (Wang, 2020 ).

## **2.18 Previous studies**

### **2.18.1 Doping Effect of CNT and Nano-Carbon in Magnesium**

#### **Diboride Bulk**

In this work Hyung was fabricated carbon nanotube (CNT) - and nano-carbon (NC)-doped  $MgB_2$  using an in-situ process in order to improve the critical current density ( $J_c$ ) at high magnetic field. Then evaluated the effects of the doped carbon content on phase formation, microstructure, and critical properties. CNT had a

diameter and length of 5–10 nm and 0.5–1 m, respectively, and NC was a sphere with diameter of 5–30 nm. The bulk  $MgB_2$  samples with  $x=0, 0.05, \text{ and } 0.1$  for NC and CNT were fabricated by pressing into pellets and then sintered at  $900^\circ\text{C}$  for 30 min. NC was more effective than CNT for carbon doping at the B site in  $MgB_2$  and, therefore, the NC-doped  $MgB_2$  samples had a lower critical temperature ( $T_c$ ) of 35.0–34.7 K than that of the CNT-doped samples (36.4–36.1 K). In addition, the  $J_c(B)$  behavior was improved when NC and CNT were doped due to doping effect. Microstructural observation suggested that the nano-sized and unreacted NC particles and the Nano domain  $MgB_2$  acted as effective flux pinning centers for the NC- and CNT-doped  $MgB_2$ , respectively (Hyung, 2009).

### **2.18 .2 Comparison of electrical and optical behaviors of MEH-PPV and MEH-PPV/CNT blend based polymer light emitting diodes**

This work done by T. A. Shahul Hameed to study the effect of incorporating nano materials to emissive polymer has been a matter of active research in polymer displays. The imbalance between electron and hole mobilities can be substantially reduced by the use of single wall carbon nano tube (SWCNT) with MEH-PPV. This work is a comparative study between two sets of devices-one with MEH-PPV and the other with a blend of MEH-PPV and carbon nanotubes as emissive materials. The electrical and optical characteristics studied by fabricating the devices show better turn on and operating performance for the device with nano blend. It will have a better switching speed due to fall in impedance and better balance between electron and mobility. (Shahu, 2011)

### **2.18.3 Properties of Single-Walled Carbon Nanotube-Based Poly(phenylene vinylene) Electroluminescent Nanocomposites**

In this paper devices with varying concentrations of single walled carbon nanotubes (SWNTs) dispersed in three derivatives of poly(p-phenylene vinylene),

and their electroluminescent properties evaluated. Increasing the concentration of SWNTs improves the electrical conductivity of the Nano composites. However, an undesired increase in the electroluminescence (EL) turn-on voltage is observed for the hybrids, possibly due to photoluminescence quenching of excisions by the SWNTs. At relatively low concentrations of SWNTs, there is an increase in the EL lifetime; in contrast, at relatively high concentrations of SWNTs, due to photoluminescence quenching by the nanotubes, significant reduction in brightness and faster degradation of the EL performance of the devices is observed inylene) Electroluminescent Nanocomposites (Abdulbaki, 2011).

#### **2.18.4 Synthesis and characterization studies of cadmium doped MgO nanocrystals for optoelectronics application**

In this paper, examination progress by using the Nano materials for several predominantly photonics device fabrication by auto combustion method, it is facile method to prepare high quality MgO and Cd doped magnesium Nano crystals, has been achieved. It is safer, easier to perform, and more cost effective than the chemical vapor. II – VI semiconductor Nano crystals are recently developed class of Nano materials whose unique photo-physical properties are helping to create a new generation in the field of photonics and microelectronics. The XRD data indicate that MgO and Cd doped magnesium nanoparticles exhibit lesser defective crystalline internal perfection. The quality of the Nano crystals was visualized by observing the surface morphology using SEM studies. Owing to all these properties the synthesized Nano crystals could be promising materials for modern materials design (Kaviyarasu, 2011).

### **2.18.5 Charge Transfer Properties in MEH-PPV/PS:MWCNTs Nanocomposites**

this work study effect of composition and annealing temperature on charge transfer properties, in a donor/acceptor nanoc Magnesium Oxide is a highly insoluble thermally stable Magnesium source suitable for glass, optic and ceramic applications. It is a hygroscopic white powder that forms magnesium hydroxide in the presence of water, historically known as magnesia alba (white mineral from Magnesia). Oxide compounds are not conductive to electricity. However, certain perovskite structured oxides are electronically conductive finding application in the cathode of solid oxide fuel cells and oxygen generation systems. They are compounds containing at least one oxygen anion and one metallic cation. composites based on poly(2-methoxy-5-(2-ethyhexyl-oxy)-p-phenylenevinylene) (MEH-PPV) and MWCNTs functionalized with Polystyrene (PS:MWCNTs), have been investigated. The quenching of photoluminescence (PL) intensity of pure MEH-PPV, by adding different amounts of functionalized carbon nanotubes, exhibits that a photoinduced charge transfer has been occurred. Charge transfer efficiency was obtained for an acceptable concentration of PS:MWCNTs about 0.5 wt% and at annealed temperature of about 80°C. Quenching efficiency studies imply that MEH-PPV/PS:MWCNTs nanocomposites reveal a high degree of PL quenching, reaching a value of  $\eta = 76.9\%$  (Chehata, 2012).

### **2.18.6 High Luminance Organic Light-Emitting Diodes with Efficient Multi-Walled Carbon Nanotube Hole Injectors**

this paper by Shengwei reported about high luminance organic light-emitting diodes by use of acid functionalized multi-walled carbon nanotube (MWCNTs) as efficient hole injector electrodes with a simple and solution processable device structure. At only 10 V, the luminance can reach nearly 50,000  $\text{cd}/\text{m}^2$  with an

external quantum efficiency over 2% and a current efficiency greater than 21 cd/A. The investigation of hole-only devices shows that the mechanism for hole injection is changed from injection limited to bulk limited because of the higher effective work function of the anode modified by the MWCNTs. We expect the enhancement of the local electric field brought about by both the dielectric inhomogeneities within the MWCNT containing anode and the high aspect ratio carbon nanotubes, improves hole injection from the anode to organic active layer at much lower applied voltage (Shi, 2014).

### **2.18. 7 Comparative Study of Deposit through a Membrane and Spin-Coated MWCNT as a Flexible Anode for Optoelectronic Applications**

The aim of this study comparative between multiwalled carbon nanotubes (MWCNTs) thin films deposited on polyethylene terephthalate (PET) substrates using spin-coating technique and deposition through a membrane. We deduce from transparence, electrical properties, and AFM image that deposition through membrane presents better properties than spin-coating method. The concentration comparison shows that the optimum result was achieved at a concentration of  $1.2 \text{ mg}\cdot\text{mL}^{-1}$  corresponding to a resistance ( $R_s$ ) of  $180 \text{ }\Omega\cdot\text{cm}^{-2}$  and an optical transparence of about 81% using a wavelength 550 nm. And will also demonstrate the use of the elaborated electrodes to fabricate the following flexible structure: PET-MWCNTs/MEH-PPV/Al. The series resistance ( $R_s$ ) and the ideality factor were calculated (Aloui, 2016).

### **2.18.8 Enhanced Structural, Thermal, and Electrical Properties of Multiwalled Carbon Nanotubes Hybridized with Silver Nanoparticle**

The aim of this study is to evaluate the structural, thermal, and electrical properties of multiwalled carbon nanotubes (MWNT) hybridized with silver nanoparticles (AgNP) obtained via chemical reduction of aqueous silver salt assisted with sodium dodecyl sulphate as stabilizing agent. Among the various metal Nano particle like silver nanoparticles has been excellent properties which make them desirable for use in biosensors, catalysts, antimicrobial agents, optical limiters, metal adsorbents and advanced composites. One of the major applications of CNT is as active elements in field-effect trans, the threshold voltage of CNT-based field emitters can reach as low as 4.6 V, unlike diamond-based ones which have a threshold voltage 40 V. For this reason appealing to integrate CNT with metal nano particle to produce CNT-based field emitters with lower threshold voltages and higher amplification factors. This study found the MWNT-Ag hybrids have enhanced the structural, thermal, and electrical characteristics of pristine MWNT using FTIR, TEM, and SEM (Yusof, 2016).

### **2.18.9 Carbon Nanotubes -Reinforcing MgO-Doped Al<sub>2</sub>O<sub>3</sub> Nanocomposites**

This work done by Iftikhar Ahmad, Uniform dispersion of CNTs during the manufacturing of CNT-reinforced MgO-doped alumina Nano composites has been achieved. The resulting of nanocomposites were appraised by combined techniques, SEM, XRD and micro hardness testing MgO doped Nano composite exhibited 14% higher hardness as compared to pressure less sintered un doped samples, and MgO-doped Nano composite manufactured by hot pressing exhibited higher mechanical properties 11% increase in density and 12% increase in hardness as

compared to those prepared by pressure less sintering. After the high temperature sintering, the CNTs not only maintained their original shape and structural characteristics but also exhibited a good interface connection with the  $\text{Al}_2\text{O}_3$  matrix. MgO and CNTs were observed to cumulatively participate in producing Nano composites with a uniform and fine grain structure (Ahmad ,2016).

#### **2.18.10 Magnesium Oxide (MgO) pH-sensitive Sensing Membrane in Electrolyte-Insulator-Semiconductor Structures with $\text{CF}_4$ Plasma Treatment**

Magnesium oxide (MgO) sensing membranes in pH-sensitive electrolyte-insulator-semiconductor, structures are fabrication on silicon substrate. To optimize the sensing capability of the membrane, the sensing material is one of the key factors in the device sensing applications, sensing membrane in the ISFET (ion-sensitive field-effect transistors) based devices plays a major role in the sensing performance, there for still some material related problems that may cloud future development of the ISFET-based sensors. The result showing using by FESEM, XRD, AFM, and SIMS it is demonstrated as good sensing film materials and the experimental data approve that the ISFET-based sensors incorporating some materials can achieve excellent sensing (Haur, 2017).

#### **2.18.11 Effect of nano-carbon percentage on properties of composite material**

This work investigated the effect of carbon nanotubes and nanoparticles in various composite materials using equations and experimental data. To determine the best amount of Nano-carbon in composite materials. The best percentage of Nano-carbon can be defined as the amount that causes an increase in some of the useful materials' properties to the highest level. These useful characteristics may be Young's modulus, tensile strength, yield strength, and fatigue life. In the presented

research, by using the experimental data and applying analytical method, equations are developed to determine the best amount of Nano carbon in composite materials including CNT, epoxy SC-15 with MWCNT-COOH, glass fiber reinforced polymer, and graphene Nano composites. Based on the results of this study using scanning electron microscopy (SEM) to microstructural investigations and Fourier Transform Infrared (FTIR) spectroscopy were used for further investigation of the effect of MWCNTs on the GFRP composite” , it appears that the best amount of Nano-carbon for every composite material is different (Anvari, 2017).

### **2.18.12 Synthesis and Characterization of Ce Doped MgO Nanocrystals**

This study demonstrates the effect of Ce on the structural, morphological, and optical properties of MgO nanostructures through a simple chemical precipitation method. Currently considerable interest in Nano crystalline oxide materials exists owing to their unusual properties, among these Magnesium Oxide (MgO) has many potential applications in almost all the areas both industrial and commercial purposes .Thermal analysis results Ce doping by MgO revealed that 450°C could be the optimum level of annealing for the harvest of pure phase of MgO. Further, the products annealed at 450°C were analyzed for their structural, optical, morphological and magnetic properties. The result obtained products using X-ray diffraction (XRD), scanning electron microscope (SEM), thermo gravimetric and differential thermal analysis (TG-DTA) and UV diffused reflectance spectroscopy (UV DRS) and FTIR spectra confirmed the formation of the MgO nanostructures. The results show that cerium atoms have been successfully incorporated into the crystal lattice of MgO with cubic structure and MgO particles thus obtained have hierarchical structures with high purity (Poonguzhali, 2017).

### **2.18. 13 Incorporating aligned carbon nanotube electrode arrays in organic thin-film transistors**

this work investigated to the effect of CNT alignment morphology in organic thin-film transistors (OTFTs). A simple method was developed to incorporate aligned SWCNT electrode arrays into an OTFT structure. The CNT structure morphology from this method was compared with an alternative method reported in the literature, that results in non-aligned carbon nanotube electrode arrays. The OTFT structure was completed employing poly[2-methoxy-5-(2-ethylhexyloxy)-1,4-phenylenevinylene] (MEH-PPV), as organic semiconductor and tested with conventional transistor output and transfer characteristics. The method employed to prepare aligned CNT electrode arrays was simple and resulted in OTFTs with lower threshold voltage and higher drain source current. The organic semiconductor MEH-PPV was chosen for its well known electroluminescent properties that aims to the possibility to study its light-emitting properties as a future work (Yi, 2019 )

### **2.18.14 Synthesis and investigation of SiO<sub>2</sub>- MgO coated MWCNTs and their potential application**

published work, multiwalled carbon nanotubes (MWCNT) coated with SiO<sub>2</sub>-MgO nanoparticles method to facilitate their incorporation into polymer matrices coated MWCNT nano composites are preparing by sol-gel technique with different multiwalled carbon nanotube content. MWCNTs have emerged as the most promising nanofiller candidate for polymer composites as of their discovery. MWCNTs with rolled graphitic layers with remarkable mechanical thermal and electrical properties can be applied as reinforcement of fiber/matrix composites to achieve improved properties. The use of MWCNTs as filler in thermoplastics such as PE, PP or polycarbonate has been widely studied. TEM, XRD and Raman investigations proved that the surface of MWCNTs was successfully coated with

inorganic nanoparticles, and after annealing, the desired SiO<sub>2</sub>–MgO layer was formed (Nemeth, 2019).

### **2.18.15 Carbon Nanotubes (CNTs)-Reinforced Magnesium-Based Matrix Composites: A Comprehensive Review**

The paper of Abazari is a comprehensive review to Carbon Nanotubes (CNTs)-Reinforced Magnesium-Based Matrix Composites. In recent years considerable attention has been attracted to magnesium because of its light weight, high specific strength, and ease of recycling. Because of the growing demand for lightweight materials in aerospace, medical and automotive industries, magnesium-based metal matrix Nano composites (MMNCs) reinforced with ceramic nanometer-sized particles, graphene Nanoplatelets (GNPs) or carbon nanotubes (CNTs) were developed. CNTs have excellent material characteristics like low density, high tensile strength, high ratio of surface-to-volume, and high thermal conductivity that makes them attractive to use as reinforcements to fabricate high-performance, and high-strength metal-matrix composites (MMCs). Reinforcing magnesium (Mg) using small amounts of CNTs can improve the mechanical and physical properties in the fabricated lightweight and high-performance nano composite. Nevertheless, the incorporation of CNTs into a Mg-based matrix faces some challenges, and a uniform distribution is dependent on the parameters of the fabricating process. The characteristics of a CNTs reinforced composite are related to the uniform distribution, weight percent, and length of the CNTs, as well as the interfacial bonding and alignment between CNTs reinforcement and the Mg-based matrix. In this review article, the recent findings in the fabricating methods, characterization of the composite's properties, and application of Mg-based composites reinforced with CNTs are studied. These include the strategies of fabricating CNT-reinforced Mg-based composites, mechanical responses, and corrosion behaviors. The present

review aims to investigate and conclude the most relevant studies conducted in the field of Mg/CNTs composites. Strategies to conquer complicated challenges are suggested and potential fields of Mg/CNTs composites as upcoming structural material regarding functional requirements in aerospace, medical and automotive industries are particularly presented (Abazari ,2020).

### **2.18.16 Graphene Oxide-Doped MgO Nanostructures for Highly Efficient Dye Degradation and Bactericidal Action**

This work objective to study effect of graphene Oxide dopant concentrations on the catalytic and antibacterial behavior of fixed amount of MgO, it has been showed effective in the areas of adsorption, catalysis for polluted water, superconducting products and antibacterial materials MgO with a large band gap of 7.8 eV have revealed a lot of interest because of the unique properties like optical, electronic and magnetic. It is an alkaline earth metal oxide with a high pH of zero charge, surface area  $\sim 250\text{--}300\text{ m}^2/\text{g}$ , and zeta potential about  $-29.89\text{V}$ . Research has found that both particle size and specific surface area are crucial factors that affect the adsorption performance. Experimental results by using FTIR, XRD, and TEM showed enhanced bactericidal efficacy of GO-MgO against G  $-ve$  (*E. coli*) relative to G  $+ve$  (*S. aureus*). In addition, synergism of GO-MgO showed enhanced bactericidal efficacy against G  $-ve$  (*E. coli*) compared to G  $+ve$  (*S. aureus*). This study explored the dopant-dependent properties of MgO Nano composites that can be employed to clean industrial polluted water and in antimicrobial applications for environmental remediation (Ikram, 2021).

# Chapter Three

## Material and Method

### 3.1 Introduction

This chapter describe the experimental details including the materials,tools and the preparation of magnesium oxide and carbon Nano tube made from (coal and soot) doping by magnesium oxide different ratio ( 0.1,0.3,0.5, 0.7 and 0.9 ) and contains the characterization techniques which used in these research.

### 3.2 Materials

The material used in this research magnesium sulphate ( $\text{MgSO}_4$  MW 246.47,Extra pure 99% ) potassium chlorate ( $\text{KClO}_3$  MW 187.55 Extra pure ),cool and soot (local samples),Nitric acid ( $\text{HNO}_3$  MW63.01),Sulphuric acid ( $\text{H}_2\text{SO}_4$  MW 246.47),Deionized water (DI) and (MEH- PPV , it is a polymers with good electrical and optical properties which can be widely applied in light-emitting diodes and photovoltaic devices).

### 3.3 Tools

The Tools used in this research Sensitive balance(model RICELAKE) , magnetic stirrer (model IKA-RH-KT ), Beaker (500-250 ml),filter paper (11cm), X-ray diffraction (XRD : model Shimadzu MAXima XRD), Fourier transforms infrared spectroscopy (FTIR : model 8100 FTIR ) and UV/VIS spectrometer(min 124 model : JENWAY 7205 ),ITO glass (It is indium tin oxide, which is characterized by its electrical conductivity, optical transparency, and easy of deposition as film.)

### 3.4 Method

#### 3.4.1 Preparation of Magnesium Oxide

Magnesium oxide samples were prepared by sol-gel technique, synthesized by using Magnesium sulfate ( $\text{MgSO}_4$ ) . Firstly, magnesium sulfate was mixed in de-ionized water by different rate. Thereafter, sodium hydroxide was added to the

magnesium sulfate solution with continuous stirring in magnetic stirrer for one hour to obtain MgO solution different ratio ( 0.1, 0.3, 0.5, 0.7 and 0.9 )

### **.3.4.2 Synthesizing carbon nanotube and doping by Magnesium Oxide**

First, 5.0g of graphite (Soot or Coal) was slowly added to a mixture of fuming nitric acid (25mℓ) and sulfuric acid (50mℓ). The mixture was kept for 30 minute. The mixture was cooled down to 5°C in an ice bath. Also 25.0g of potassium chlorate was slowly added to the solution while stirring for 30 minutes. Since a lot of heat was produced while adding potassium chlorate into the mixture, special care during this step is needed to smear out temperature effect. The solution was heated up to 70°C for 24 hours and was then placed in air for 3 days. Most of graphite was precipitated on the bottom but some reacted carbons were floating. The floating carbon materials were transferred into DI water (1ℓ). After stirring for 1 hour, the solution was immediately filtrated and the sample was dried to obtain by above method CNT were doped by Magnesium Oxide (MgO) preparing by sol gel method in different ratio(0.1, 0.3, 0.5, 0.7 and 0.9).





### 3.4.3 Spin coating of Carbon Nano Tube (CNT) and MEH-PPV

Fabrication of the device was through spin casting of Carbon Nano Tube (CNT) from (Soot and Coal) and doping by Magnesium Oxide (Mg O) in different molar and MEH-PPV .This category of device exhibits current and voltage turn on below. By spin coating of single layer and double layers for Poly (2-methoxy, 5-(2-ethylhexoxy)-1, 4- phenylene-vinylene (MEH- PPV) and carbon nanotube used ITO glass as cathode .

After preparing samples using X-ray diffraction (XRD) technique for the determination of the total crystalline structure of nanotubes.It used Cu K $\alpha$  radiation ( $\lambda = 0.15418$  nm) at a rate of 0.06 /second. The XRD pattern was recorded over a  $2\theta$  interval of  $10^\circ$  to  $50^\circ$ , and worked at 40 kV and current of 30 mA.Whether functional groups were present or not was detected using Fourier transform infrared spectrum (FT-IR ),were recorded in transmission mode apparatus in the 400 and 4000  $cm^{-1}$  region and to obtain the optical properties (absorbance, transmission, reflection, absorption coefficient, extinction coefficient and optical energy band gap) using UV-Visible min 1240 spectrophotometer .To apply this martial as diode multilayer (IV curve) Using MEH-PPV device. Finally, the results were analyzed by using the Origin software.

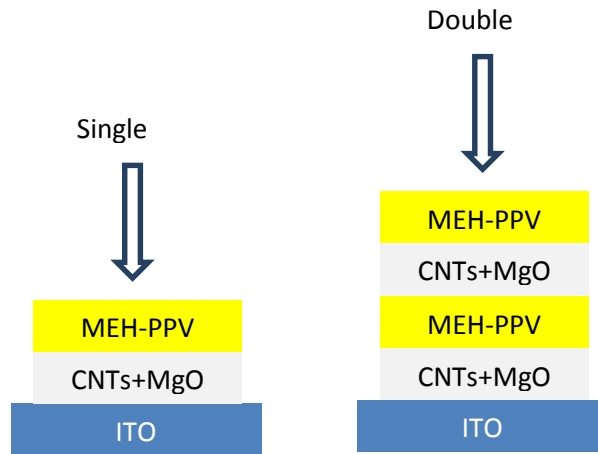


Figure (3.1) spin casting of Carbon Nano Tube (CNT) and MEH-PPV

## Characterization Techniques

the characterization techniques used in this research :

### 3.5.1 X-ray diffraction technique (XRD)

X-ray diffraction (XRD) is a powerful nondestructive technique for characterizing crystalline materials. It provides information on structures, phases, preferred crystal orientations (texture), and other structural parameters, such as average grain size, crystallinity strain and crystal defects. X-ray diffraction peaks were produced by constructive interference of a monochromatic beam of X-rays scattered at special angles from each set of lattice planes in a sample. The peak intensities were determined by the distribution of atoms within the lattice. Consequently, the X-ray diffraction pattern of periodic atomic arrangements in a given material. The interaction of the incident rays with the sample produces constructive interference (and a directed ray) when conditions satisfy Bragg's law (Bunaciu, 2015).



Figure (3.1) XRD instrument

### 3.5.2 Fourier transforms infrared spectroscopy (FTIR)

Fourier transforms infrared spectroscopy (FTIR) was used to study the structural properties. It is used to measure the vibrational frequencies of bonds in the molecule, the vibrational energy levels of sample molecules transfer from ground state to excited state. The frequency of the absorption peak is determined by the vibrational energy gap. The number of absorption peaks is related to the number of vibrational freedom of the molecule. The intensity of absorption peaks is related to the change of dipole moment and the possibility of the transition of energy levels. Therefore, by analyzing the infrared spectrum, one can readily obtain abundant structure information of a molecule (Shalini, 2012)



Figure (3-2) FTIR Spectroscopy

### 3.5.3 UV-Vis Spectroscopy

UV-Vis Spectroscopy is an analytical method used to measure the absorbance of ultra-violet or visible radiation through an analytic. The molecular absorption of the analytic corresponds to both excitation of valence electrons and excitation of electrons in different atomic orbitals. UV-Vis Spectroscopy is an effective technique for both qualitative and quantitative analysis of organic and inorganic compounds to study the optical properties of materials the wavelength range (200-800nm) (den ,2006)



Figure (3.3) UV-Vis Spectroscopy

### 3.5.4 I-V characteristics multilayers

The diode circuit consists of a voltage source, an ammeter to calculate the current, a voltmeter to calculate the voltage, a rheostat and a multi-layer diode. The results are recorded by stabilizing the initial voltage and then changing the rheostat and recording the voltage and current reading to give the circuit curve .

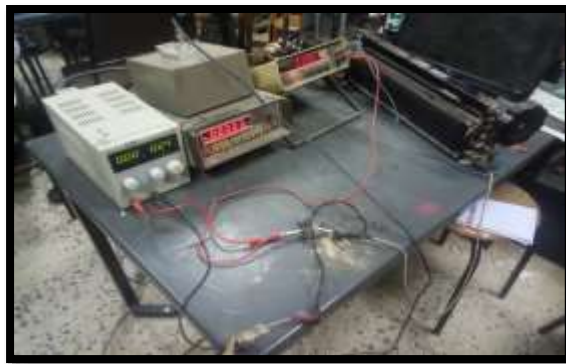


Figure (3.5) I-V Circuit

## Chapter Four

### Results and Discussion

#### 4.1 Introduction

In this chapter the main results that have been obtained from the experiments made of Carbon Nano Tube (CNT) from (Soot and Coal) and doping by Magnesium Oxide (MgO) in different ratio (0.1, 0.3, 0.5, 0.7 and 0.9) . The data of X-ray diffraction (XRD) have been to gated crystal structure and lattice parameters of samples, the FT-IR data have been carried to investigate the chemical bonds within atoms, and the data of UV-visible used to evaluate the optical parameters. At last to apply this now martial as diode malty layers (IV curve).

#### 4.2.1 XRD Results of Carbon Nano Tube (CNT) dopped by (MgO)

The result spectrum show in fig (4.1- 4.5) the XRD of all Carbon Nano Tube (CNT) from (Soot and Coal) and doping by Magnesium Oxide (MgO) in different ratio (0.1, 0.3, 0.5, 0.7 and 0.9)

#### Soot Results

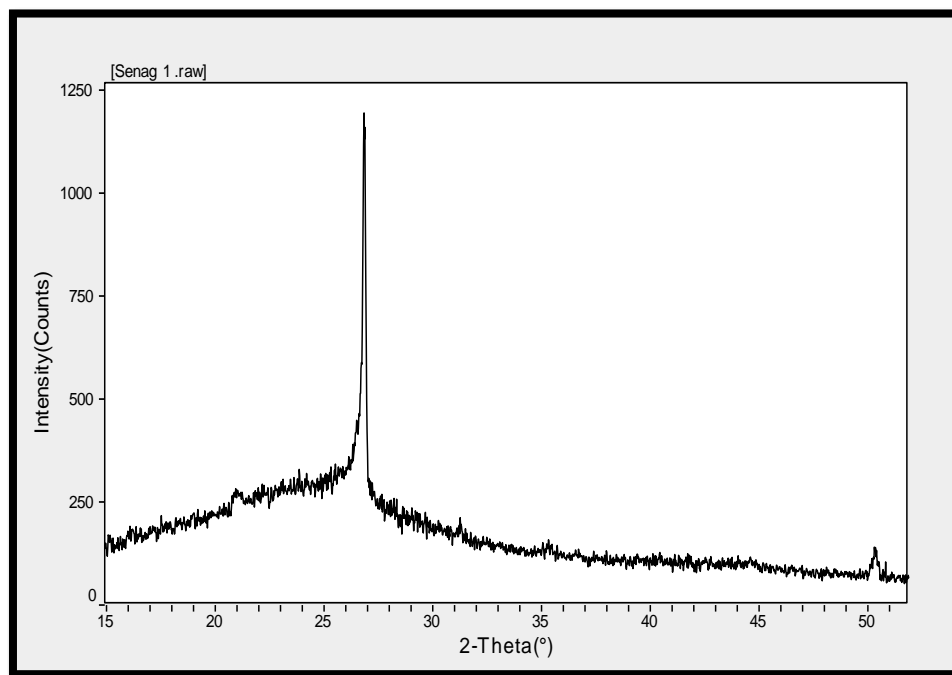


Fig (4.1) XRD spectrum of Carbon Nano Tube (CNT) from Soot and doping by Magnesium Oxide (MgO) 0.1 ratio

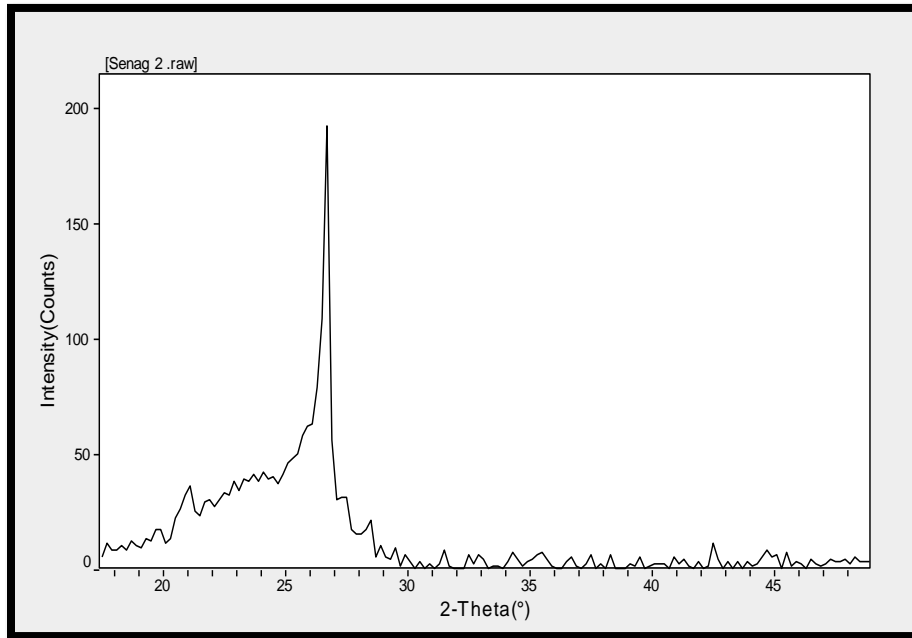


Fig (4.2) XRD spectrum of Carbon Nano Tube (CNT) from Soot and doping by Magnesium Oxide (MgO) 0.3 ratio

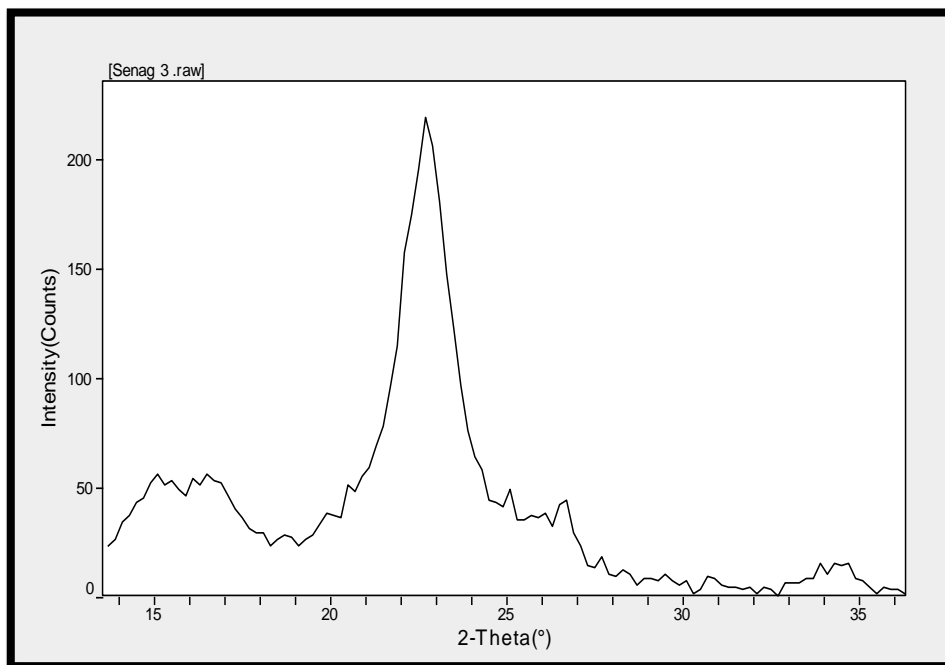


Fig (4.3) XRD spectrum of Carbon Nano Tube (CNT) from Soot and doping by Magnesium Oxide (MgO) 0.5 ratio

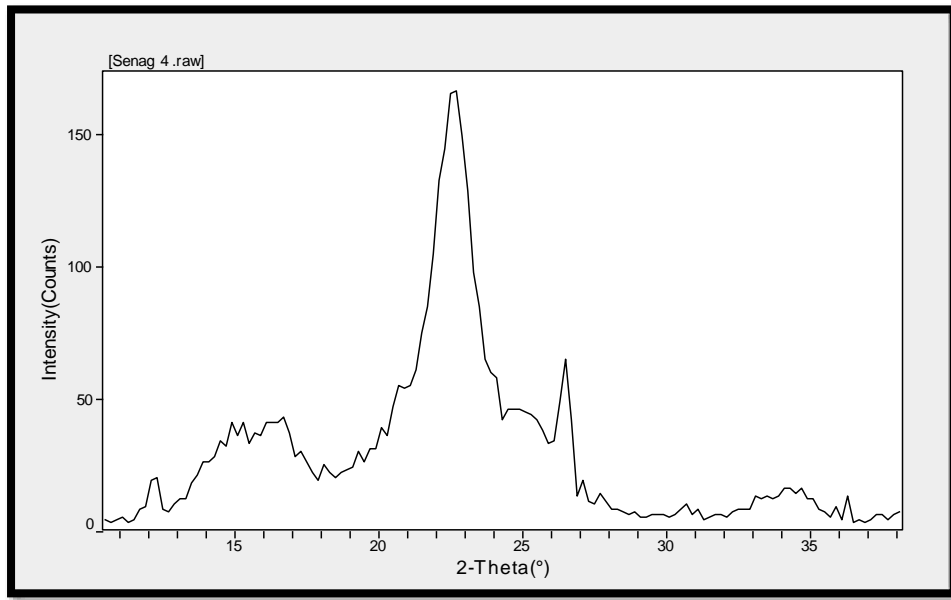


Fig (4.4) XRD spectrum of Carbon Nano Tube (CNT) from Soot and doping by Magnesium Oxide (MgO) 0.7 ratio

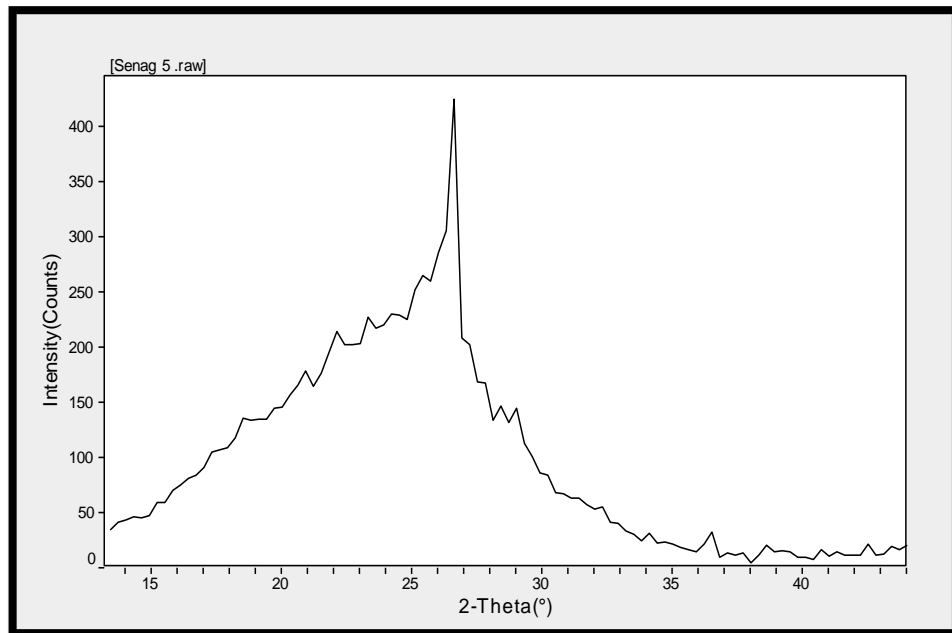


Fig (4.5) XRD spectrum of Carbon Nano Tube (CNT) from Soot and doping by Magnesium Oxide (MgO) 0.9 ratio

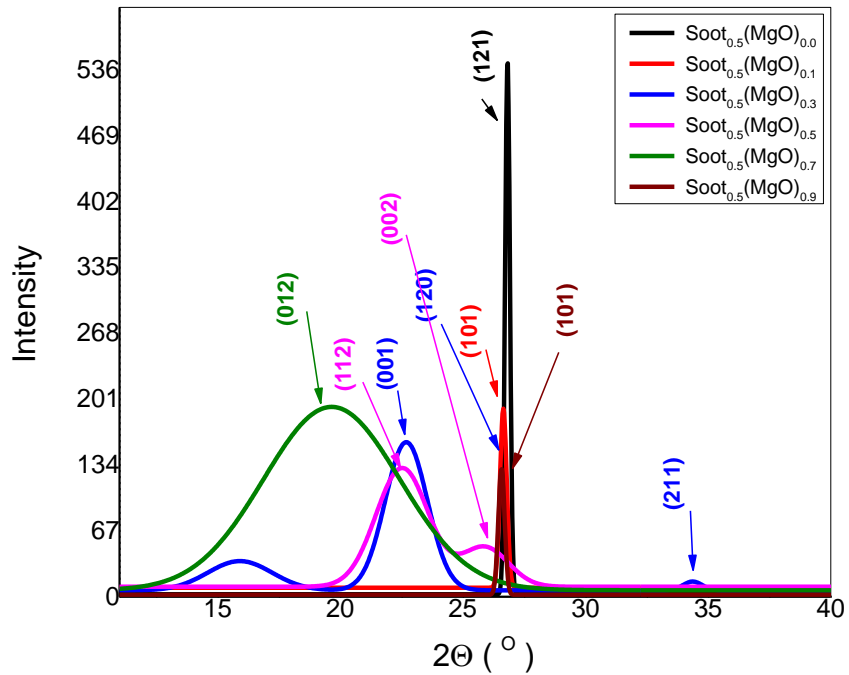


Fig (4.6) XRD spectrum of Carbon Nano Tube (CNT) samples that made from Soot doping by Magnesium Oxide (MgO) (0.1, 0.3, 0.5, 0.7 and 0.9) ratio

Table (4.1) Calculate Lattice Constants from Peak Locations and Miller Indices of Carbon Nano Tube (CNT) samples that made from Soot doping by Magnesium Oxide (MgO) (0.1, 0.3, 0.5, 0.7 and 0.9) ratio using mdi-jad programe .

No	$2\theta$ (°)	$d$ (Å <sup>0</sup> )	FWHM	$X_s$ (nm)	h k l	$\delta$ (mg.cm <sup>-3</sup> )
S1	26.500	3.3608	0.442	07.9	1 2 1	4.7179
S2	26.641	3.3532	0.197	08.2	1 0 1	3.6697
S3	22.500	3.3483	0.919	08.9	0 0 1	3.7849
S4	22.302	3.3430	0.905	19.0	0 1 2	3.2114
S5	26.668	3.3321	0.270	32.5	0 1 2	2.9424
S6	26.620	3.3258	0.250	35.6	1 0 1	2.8161

## coal Result:

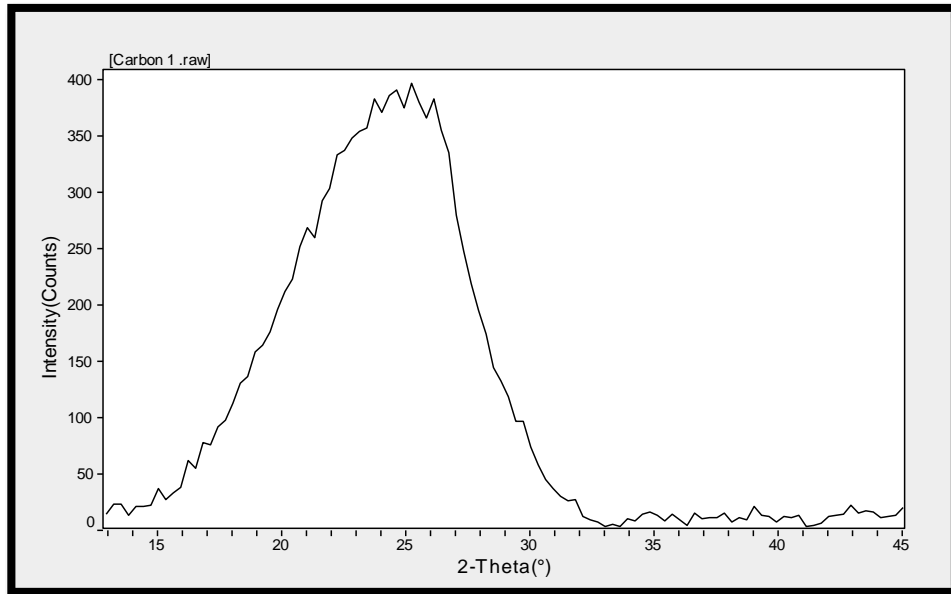


Fig (4.7) XRD spectrum of Carbon Nano Tube (CNT) from Coal and doping by Magnesium Oxide (MgO) 0.1 ratio

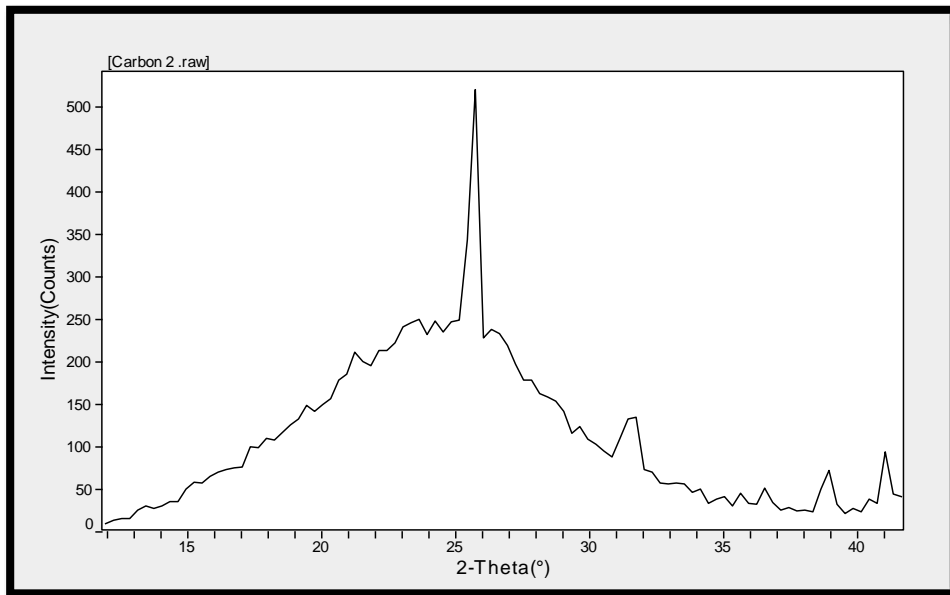


Fig (4.8) XRD spectrum of Carbon Nano Tube (CNT) from Coal and doping by Magnesium Oxide (MgO) 0.3 ratio

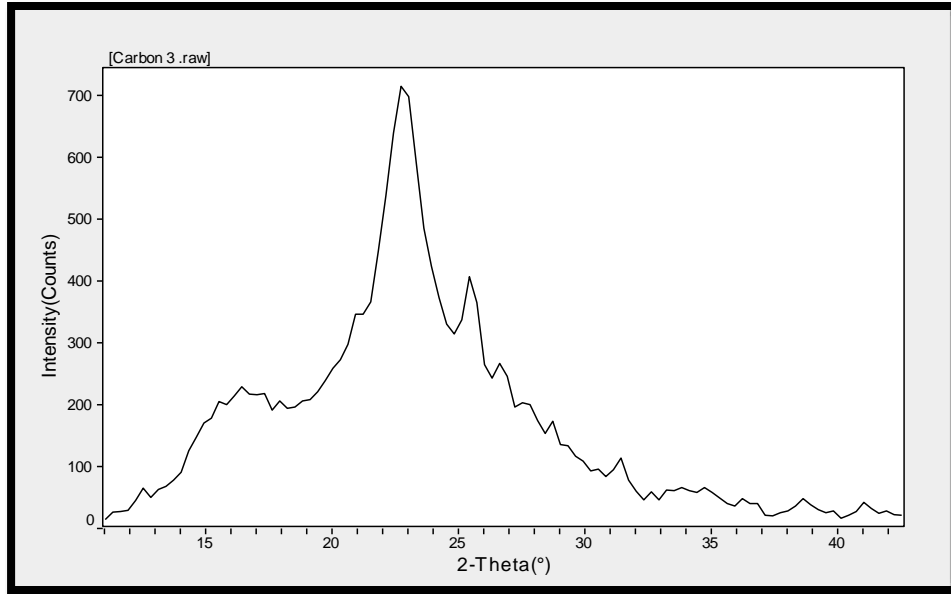


Fig (4.9) XRD spectrum of Carbon Nano Tube (CNT) from Coal and doping by Magnesium Oxide (MgO) 0.5 ratio

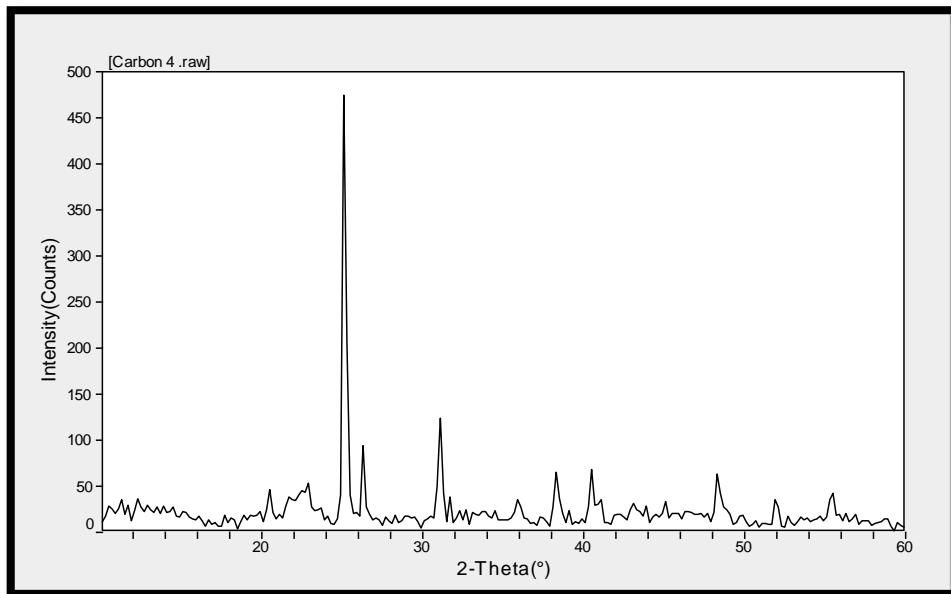


Fig (4.10) XRD spectrum of Carbon Nano Tube (CNT) from Coal and doping by Magnesium Oxide (MgO) 0.7 ratio

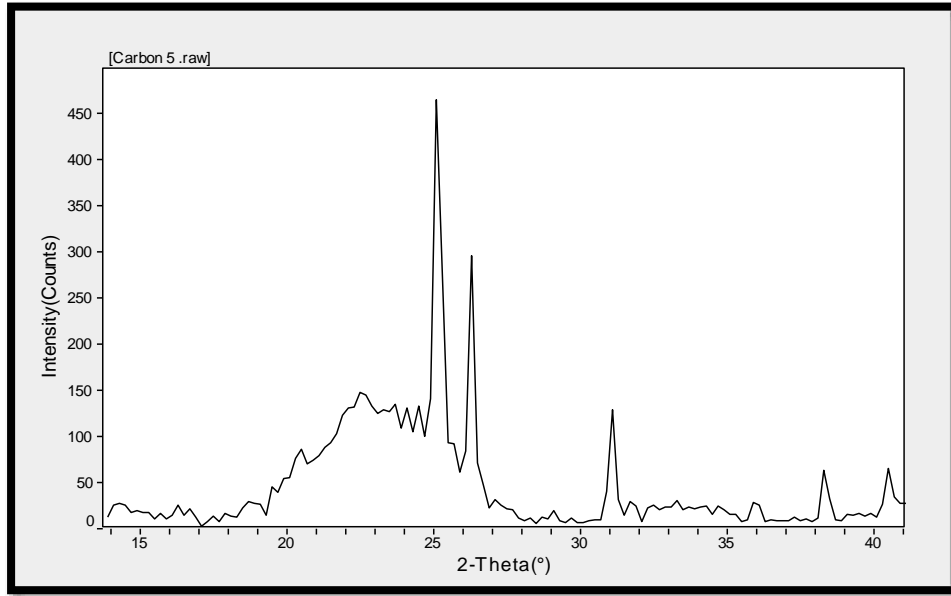


Fig (4.11) XRD spectrum of Carbon Nano Tube (CNT) from Coal and doping by Magnesium Oxide (MgO) 0.9 ratio

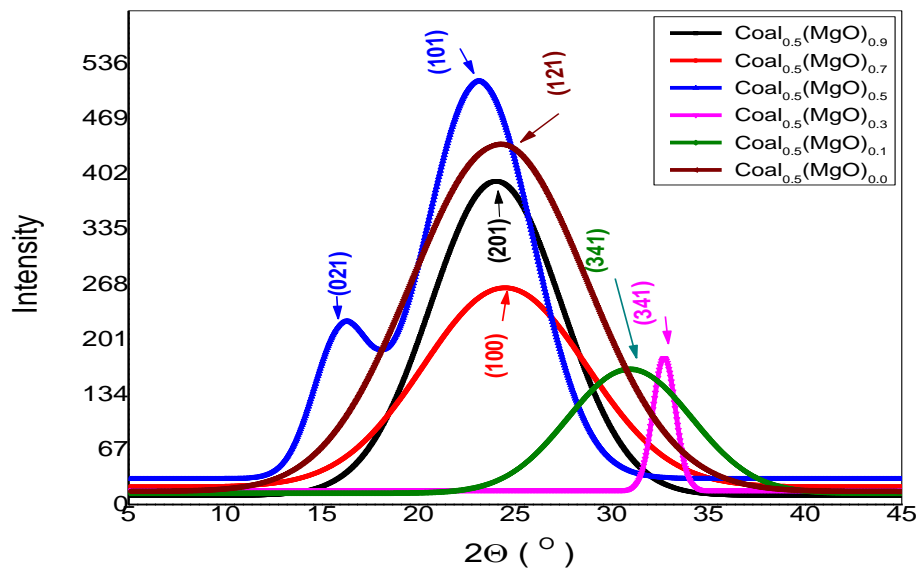


Fig (4.12) XRD spectrum of Carbon Nano Tube (CNT) samples that made from Coal doping by Magnesium Oxide (MgO) (0.1, 0.3, 0.5, 0.7 and 0.9) ratio

Table (4.2) Calculate Lattice Constants from Peak Locations and Miller Indices of Carbon Nano Tube (CNT) samples that made from Coal doping by Magnesium Oxide (MgO) (0.1, 0.3, 0.5, 0.7 and 0.9) ratio

No	2θ ( ° )	d ( Å )	FWHM	X <sub>s</sub> ( nm )	h k l	δ (mg.cm <sup>-3</sup> )
C1	24.115	3.42446	0.198	47.7	2 0 1	6.4267
C2	24.423	3.4685	0.180	54.4	1 0 0	4.1522
C3	16.240	3.8655	0.732	61.2	0 2 1	3.7849
C4	32.692	3.5394	0.168	67.5	0 1 2	3.2114
C5	30.885	3.3399	0.190	70.3	3 4 1	2.8746
C6	24.279	3.4760	0.178	75.1	1 2 1	0.1752

#### 4.2.2 XRD Discussion of Carbon Nano Tube (CNT) doping by (MgO)

The crystal structure of all samples characterized at room temperature using a Philips PW1700 X-ray diffract meter (operated at 40 kV and current of 30 mA) and samples were scanned between 5° and 25° at a scanning speed of 0.06 ° C/s using Cu Kα radiation with  $\lambda = 1.5418\text{Å}$ . The representative XRD charts of all Carbon Nano Tube (CNT) samples that made from (Soot and Coal) doping with Magnesium Oxide (MgO) (0.1, 0.3, 0.5, 0.7 and 0.9) ratio as show from fig (4.1) to fig(4.6) for the made with Soot and fig (4.7) to fig (4.12) that samples made from Coal. Miller indices provided in the fig (6) and all peaks determine transformation of Carbon Nano Tube (CNT) samples that made from Soot doping by Magnesium Oxide (MgO) (0.1, 0.3, 0.5, 0.7 and 0.9). ratio crystallites with (Monoclinic – primitive) crystal structure for the sample Soot<sub>0.5</sub> (MgO)<sub>0.0</sub> (a=21.41, b=7.2792 and c=9.5221/  $\alpha = 90^\circ$ ,  $\beta = 97.945^\circ$  and  $\gamma = 90^\circ$ ), when the sample be Soot<sub>0.5</sub> (MgO)<sub>0.1</sub> (a = b= 2.456 and c = 20.088 /  $\alpha = \beta = 90^\circ$  and  $\gamma = 120^\circ$ ) with (Hexagonal – primitive) crystal structure , and the molar crystallites with (Orthorhombic – primitive) crystal structure for the sample Soot<sub>0.5</sub> (MgO)<sub>0.3</sub> (a = 12.372 , b=37.1

and  $c = 3.954$  /  $\alpha = \beta = \gamma = 90^\circ$ ), and for sample Soot<sub>0.5</sub> (MgO)<sub>0.5</sub> ( $a = 9.736$ ,  $b = 8.469$  and  $c = 12.777$  /  $\alpha = 90^\circ$ ,  $\beta = 90.56^\circ$  and  $\gamma = 90^\circ$ ) with (Monoclinic – primitive) crystal structure, the molar crystallites with (Monoclinic – primitive) crystal structure for the sample Soot<sub>0.5</sub> (MgO)<sub>0.7</sub> ( $a = 6.9754$ ,  $b = 12.764$  and  $c = 6.962$  /  $\alpha = 91.16^\circ$ ,  $\beta = 90.32^\circ$  and  $\gamma = 83.22^\circ$ ) and the last them Molar crystallites with (Monoclinic – primitive) crystal structure for the sample Soot<sub>0.5</sub> (MgO)<sub>0.9</sub> ( $a = b = 2.456$  and  $c = 20.088$  /  $\alpha = \beta = 90^\circ$  and  $\gamma = 120^\circ$ ). Table (3) shows the XRD parameters of Carbon Nano Tube (CNT) samples that made from Soot doping by Magnesium Oxide (MgO) (0.1, 0.3, 0.5, 0.7 and 0.9) molar at various crystalline orientations. When we describe the relation between the rated molar Magnesium Oxide (MgO) and density of samples, we showing that decreasing the density by increasing the molar of Magnesium Oxide (MgO), and the crystals size increasing with increases molar as calculated from table (4.1). And for the representative XRD charts of all Carbon Nano Tube (CNT) samples that made from Coal doping by Magnesium Oxide (MgO) (0.1, 0.3, 0.5, 0.7 and 0.9) Molar as show in fig (4.12). The miller indices provided in the figure (4.12) and all peaks determine transformation of Carbon Nano Tube (CNT) samples that made from coal doping by Magnesium Oxide (MgO) (0.1, 0.3, 0.5, 0.7 and 0.9) ratio. Crystallites with (Tetragonal – primitive) crystal structure for the sample Coal<sub>0.5</sub> (MgO)<sub>0.0</sub> ( $a = b = 7.46$  and  $c = 8.61$  /  $\alpha = \beta = \gamma = 90^\circ$ ), when the sample be Coal<sub>0.5</sub> (MgO)<sub>0.1</sub> ( $a = b = c = 4.152$  /  $\alpha = \beta = \gamma = 90^\circ$ ) with (Cubic – primitive) crystal structure, and the molar crystallites with (Monoclinic – primitive) crystal structure for the sample Coal<sub>0.5</sub> (MgO)<sub>0.3</sub> ( $a = 7.1986$ ,  $b = 7.9393$  and  $c = 17.39$  /  $\alpha = 90^\circ$ ,  $\beta = 90.6204^\circ$  and  $\gamma = 90^\circ$ ), and for sample Coal<sub>0.5</sub> (MgO)<sub>0.5</sub> ( $a = b = 5.39$  and  $c = 46.52$  /  $\alpha = \beta = 90^\circ$  and  $\gamma = 120^\circ$ ) with (Hexagonal – primitive) crystal structure, the molar crystallites with (Triclinic – primitive) crystal structure for the sample Coal<sub>0.5</sub> (MgO)<sub>0.7</sub> ( $a = 6.485$ ,  $b = 6.415$

and  $c = 16.8$  /  $\alpha = 90.11^\circ$ ,  $\beta = 95.91^\circ$  and  $\gamma = 90.95^\circ$ ) and the last them Molar crystallites with (Orthorhombic – primitive) crystal structure for the sample Coal  $_{0.5}(\text{Mg O})_{0.9}$  ( $a = 11.35$ ,  $b = 24.08$  and  $c = 4.1398$  /  $\alpha = \beta = \gamma = 90^\circ$ ). Table (4) shows the XRD parameters of Carbon Nano Tube (CNT) samples that made from Coal doping by Magnesium Oxide (MgO) (0.1, 0.3, 0.5, 0.7 and 0.9) ratio at various crystalline orientations. When we describe the relation between the rated molar Magnesium Oxide (MgO) and density of samples, we showing that decreasing the density by increasing the molar of Magnesium Oxide (MgO), and the crystals size increasing with increases ratio as calculated from table (4.2).

### 4.3.1 FTIR Results of Carbon Nano Tube (CNT) doping by (MgO)

After made Carbon Nano Tube (CNT) from (Soot and Coal) and doping by Magnesium Oxide (MgO) in different ratio (0.1, 0.3, 0.5, 0.7 and 0.9) used Fourier transforms infrared spectroscopy (FTIR) to study the structural properties as shown in the results

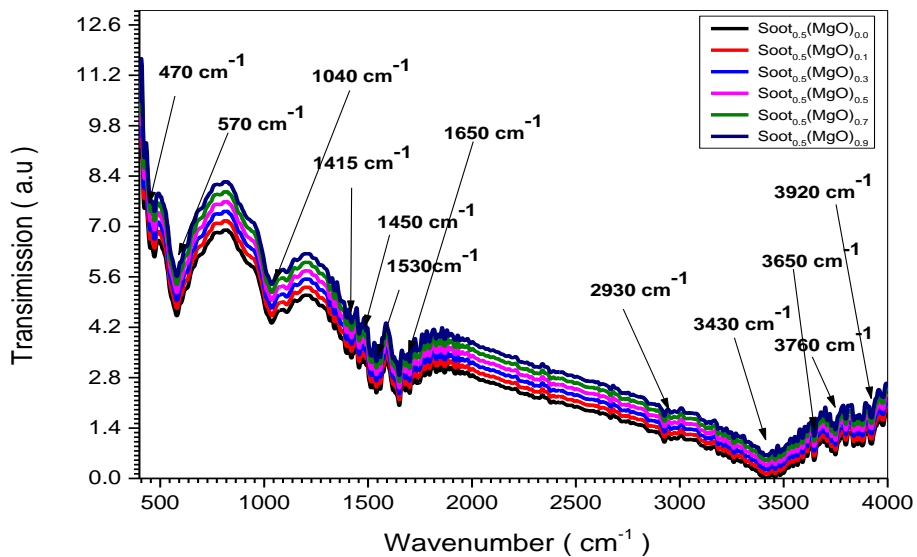


Fig (4.13) IR spectrum of CNTs from (Soot) + Magnesium Oxide (MgO) (0.1, 0.3, 0.5, 0.7 and 0.9) ratio samples

Table (4.3) Table of Characteristic IR of CNTs from (Soot) + Magnesium Oxide (MgO) (0.1, 0.3, 0.5, 0.7 and 0.9) ratio samples

No	Wavenumber (cm <sup>-1</sup> )	Functional Group Names	Type of Vibration	Referance
1	470	meta disubstituted aromatic	C-H bend patterns for aromatics	650-1000
2	570	alkyl halides	C-Br stretch	515-690
3	1040	Esters	(C-O Stretch)	1000-1320
4	1415	Alkanes	C-H bend	1450-1470
5	1450	Aromatic Rings	C-C=C Asymmetric Stretch	1400-1500
6	1530	Aromatic Compounds	C=C stretch	1400-1500
7	1650	Carboxylic Acids	C=O Stretch	1640-1680
8	2930	Alkanes	C-H stretch	2850-3000
9	3430	Phenols & Alcohols	Hydrogen-bonded O-H Stretch	3200-3500
10	3650	Alcohols	O-H stretch (strong and broad)	3500-4000
11	3760	Alcohols	O-H stretch	3500-+4000
12	3920	alkynes (terminal)	-C≡C-H: C-H stretch	3500-4000

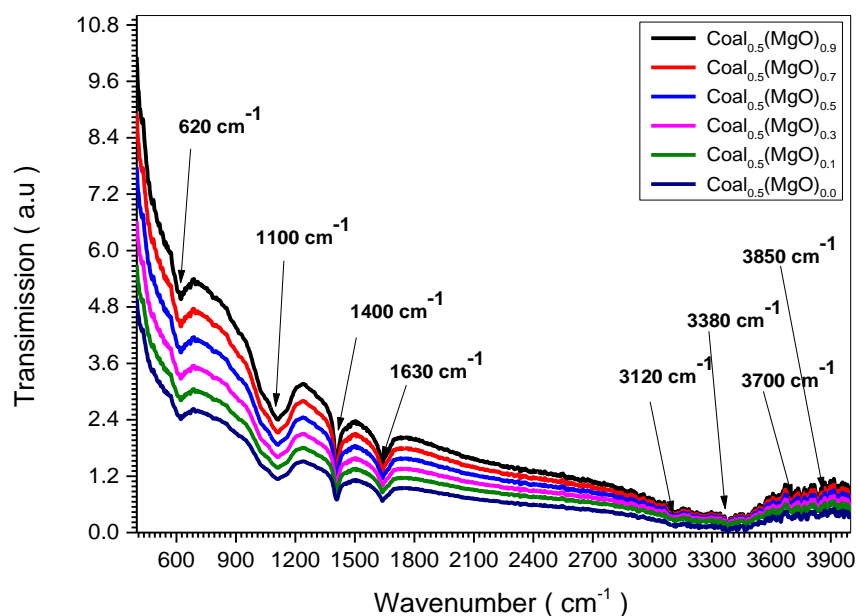


Fig (4.14) IR spectrum of CNTs from (Coal) + Magnesium Oxide (MgO) (0.1, 0.3, 0.5, 0.7 and 0.9) ratio samples

Table (4.4) Table of Characteristic IR of CNTs from (Coal) + Magnesium Oxide (MgO) (0.1, 0.3, 0.5, 0.7 and 0.9) ratio samples

No	Wavenumber (cm <sup>-1</sup> )	Functional Group Names	Type of Vibration	Referance
1	620	alkyl halides	C-Br stretch	515-690
2	1100	Esters	(C-O Stretch)	1000-1320
3	1400	Aromatic	C-H stretch	1400-1500
4	1630	Alkenes	C=C stretch	1580-1650
5	3120	Amines—Primary	N-H Stretch	3250-3400
6	3650	Alcohols	O-H stretch (strong and broad)	3500-4000
7	3700	Alcohols	O-H stretch	3500-4000
8	3850	alkynes (terminal)	-C ≡ C-H: C-H stretch	3500-4000

#### 4.3.2 FTIR Discussion of Carbon Nano Tube (CNT) doping by (MgO)

Fourier Transform Infrared spectroscopy is a technique used to measure the vibrational frequencies of bonds in the molecule. The FTIR spectra of CNTs from (Soot) + Magnesium Oxide (MgO) (0.1, 0.3, 0.5, 0.7 and 0.9) ratio samples is shown in Fig (4.13). The strong intensity peak at 3920 cm<sup>-1</sup> assigned to alkynes (terminal) -C ≡ C-H: C-H stretch, at 3760 cm<sup>-1</sup> assigned to O-H stretch vibration of alcohol group, the band at 3650 cm<sup>-1</sup> assigned to Alcohols group (O-H stretch - strong and broad) vibration. Peak at 3430 cm<sup>-1</sup> assigned to Phenols & Alcohols (Hydrogen-bonded O-H Stretch) while the very intense peak positioned at 2930 cm<sup>-1</sup> revealed the presence of (C-H stretch) stretching for Alkenes. The characteristic peaks of C=O stretch positioned from 1650 cm<sup>-1</sup> vibration of carboxylic acids. The peaks positioned at 1530 cm<sup>-1</sup> observed due to C=C stretch vibration of aromatic compounds. The intensity peak at 1450 cm<sup>-1</sup> assigned to Aromatic Rings C-C=C Asymmetric Stretch vibration, at 1415 cm<sup>-1</sup> assigned to C-H bend vibration of alkanes group, the band at 1040 cm<sup>-1</sup> assigned to Esters group

(C-O Stretch)vibration. Peak at  $570\text{ cm}^{-1}$  assigned to alkyl halides C-Br stretch , while the very intense peak positioned at  $470\text{ cm}^{-1}$  revealed the presence of (C-H bend patterns for aromatics) stretching for meta ( MgO) disubstituted aromatic. All this results as shown in table (4.3) .The FTIR spectra of CNTs from (Coal) + Magnesium Oxide (MgO) (0.1, 0.3, 0.5, 0.7 and 0.9) ratio samples is shown in Fig (4.14).The strong intensity peak at  $3850\text{ cm}^{-1}$  assigned to alkynes (terminal)  $\text{-C}\equiv\text{C-H}$ : C-H stretch, at  $3700\text{ cm}^{-1}$  assigned to O-H stretch vibration of alcohol group, the band at  $3380\text{ cm}^{-1}$  assigned to Phenols & Alcohols (Hydrogen-bonded O-H Stretch) vibration. Peak at  $3120\text{ cm}^{-1}$  assigned to Amines Primary N-H Stretch,while the very intense peak positioned at  $1630\text{ cm}^{-1}$  revealed the presence of (C=C stretch) stretching for Alkenes.The characteristic peaks of C-H stretch positioned from  $1400\text{ cm}^{-1}$  vibration of aromatic. The peaks positioned at  $1100\text{ cm}^{-1}$  observed due to C-O Stretch vibration of esters compounds.The intensity peak at  $620\text{ cm}^{-1}$  assigned to alkyl halides C-Br stretch vibration. All this results were show in table (4.4).

#### **4.3.1 UV-Vis Results of Carbon Nano Tube (CNT) doping by (MgO)**

After made Carbon Nano Tube (CNT) from (Soot and Coal) and doping by Magnesium Oxide (MgO) in different ratio (0.1, 0.3, 0.5, 0.7 and 0.9) was used UV-VS mini 1240 spectrophotometer to study the optical properties (absorbance, transmission, reflection, absorption coefficient, extinction coefficient and optical energy band gap) as shown in the results

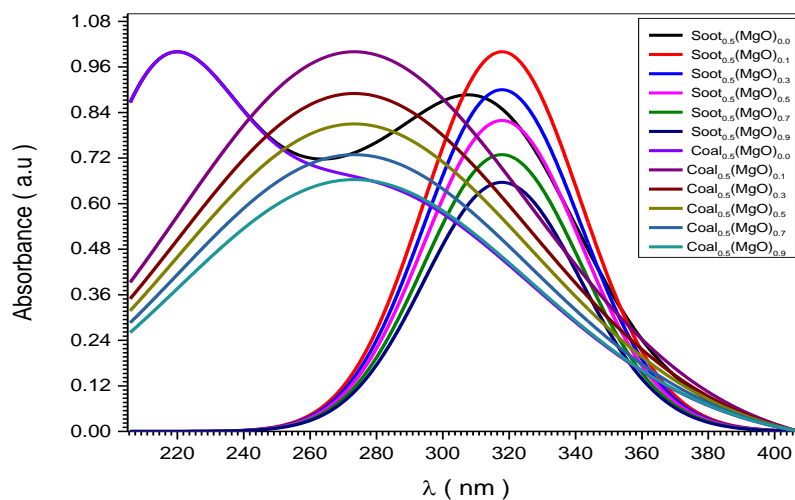


Fig (4.15) the relation between absorbance and wavelngths of (Soot and Coal) + Magnesium Oxide (MgO) (0.1, 0.3, 0.5, 0.7 and 0.9) ratio samples

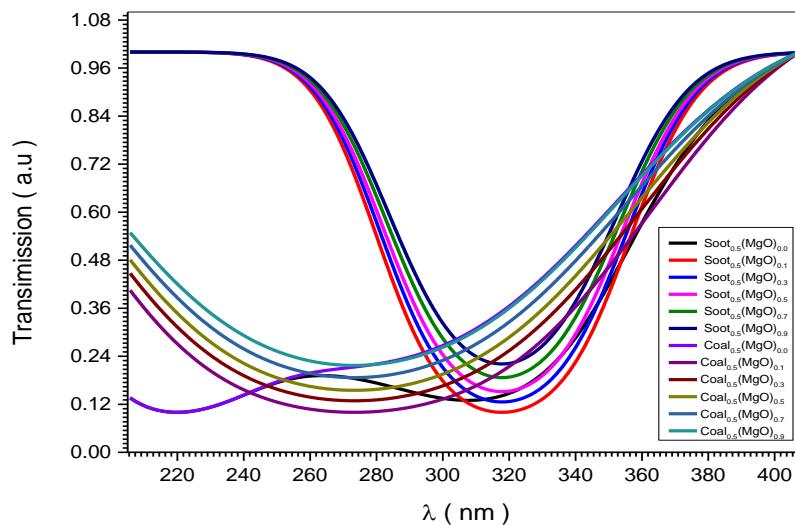


Fig. (4.16) Shown the relation between transmission and wavelngths for (Soot and Coal) +Magnesium Oxide (MgO) (0.1, 0.3, 0.5, 0.7 and 0.9) ratio samples

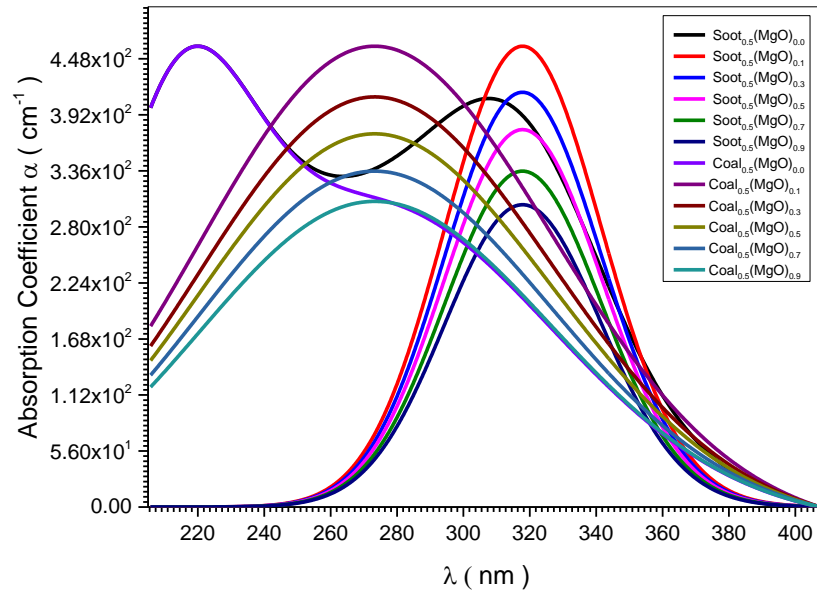


Fig (4.17) the relation between absorption coefficient and wavelengths of (Soot and Coal) + Magnesium Oxide (MgO) (0.1, 0.3, 0.5, 0.7 and 0.9) ratio samples

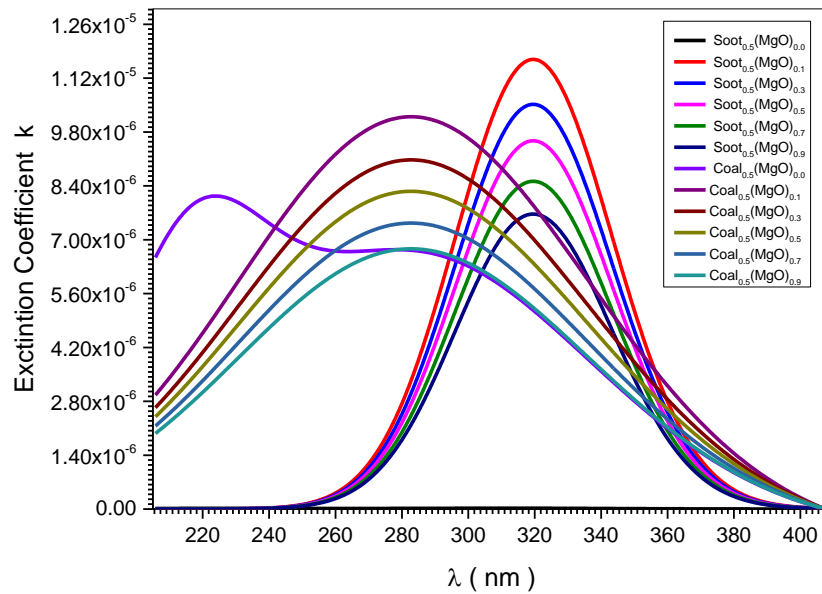


Fig (4.18) the relation between extinction coefficient and wavelengths of (Soot and Coal) + Magnesium Oxide (MgO) (0.1, 0.3, 0.5, 0.7 and 0.9) ratio samples

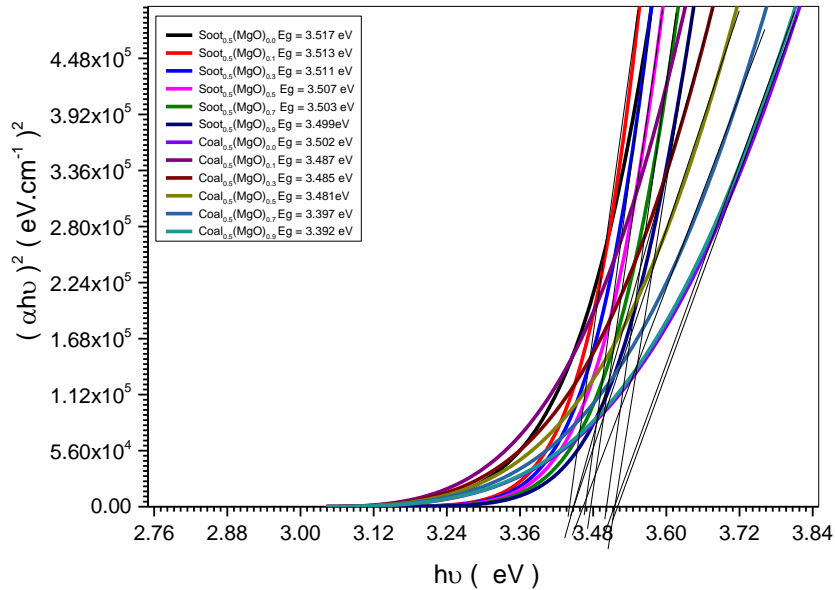


Fig (4.19) the optical energy band gap of (Soot and Coal) + Magnesium Oxide (MgO) (0.1, 0.3, 0.5, 0.7 and 0.9)ratio samples

### 4.3.2 UV-Vis Discussion of Carbon Nano Tube (CNT) doping by (MgO)

From the Fig (4.15 – 4.19) we found the behavior of (Soot and Coal) doping by Magnesium Oxide (MgO) (0.1, 0.3, 0.5, 0.7 and 0.9)ratio samples studied using UV-VS min 1240 spectrophotometer. figure (4.15) Shows the relation between absorbance and wavelengths for (Soot and Coal) doping by Magnesium Oxide (MgO) (0.1, 0.3, 0.5, 0.7 and 0.9) ratio samples, for Soot samples the rapid decrease absorption at wavelengths 317 nm corresponding photon energy 3.912 eV by doping increase .For Coal samples the rapid decrease a absorption at wavelengths 272 nm corresponding photon energy 4.559 eV by doping increase.The absorption coefficient ( $\alpha$ ) of the (Soot and Coal) doping by Magnesium Oxide (MgO) (0.1, 0.3, 0.5, 0.7 and 0.9) ratio samples were found from the following equation  $\alpha = \frac{2.303xA}{t}$  where (A) is the absorbance and (t) is the

optical length in the samples. Fig (4.16) shown the plot of  $(\alpha)$  with wavelength  $(\lambda)$  of (Soot and Coal) doping by Magnesium Oxide (MgO) (0.1, 0.3, 0.5, 0.7 and 0.9) ratio samples, which obtained that the value of  $\alpha = 4.62 \times 10^2 \text{ cm}^{-1}$  for Soot<sub>0.5</sub>(MgO)<sub>0.1</sub> sample in the U.V region (317 nm) but for Soot<sub>0.5</sub>(MgO)<sub>0.9</sub> sample equal  $3.02 \times 10^2 \text{ cm}^{-1}$  at the same wavelength, and for the Coal<sub>0.5</sub>(MgO)<sub>0.1</sub> sample the absorption coefficient equal  $4.62 \times 10^2 \text{ cm}^{-1}$  at 272 nm, but for Coal<sub>0.5</sub>(MgO)<sub>0.9</sub> sample equal  $3.07 \times 10^2 \text{ cm}^{-1}$  at the same wavelength, this means that the transition must corresponding to indirect electronic transition, and the properties of this state are important since they are responsible for electrical conduction. Also, fig (4.16) shows that the value of  $(\alpha)$  for all (Soot and Coal) doping by Magnesium Oxide (MgO) (0.1, 0.3, 0.5, 0.7 and 0.9) ratio samples decrease while doping increased. Extinction coefficient (K) was calculated using the relation  $= \frac{\alpha \lambda}{4\pi}$ . The variation of the extinction coefficient (K) values as a function of  $(\lambda)$  are shown in fig (4.17) for (Soot and Coal) doping by Magnesium Oxide (MgO) (0.1, 0.3, 0.5, 0.7 and 0.9) ratio samples and it is observed that the spectrum shape of (K) as the same shape of  $(\alpha)$ . The extinction coefficient (K) for (Soot and Coal) doping by Magnesium Oxide (MgO) (0.1, 0.3, 0.5, 0.7 and 0.9) ratio samples, in fig (4.17) obtained the value of (K) for the Soot samples at the (317 nm) wavelength was depend on the samples treatment method, where the value of (K) at 317 nm for Soot<sub>0.5</sub>(MgO)<sub>0.1</sub> sample equal  $1.17 \times 10^{-5}$  while for other sample Soot<sub>0.5</sub>(MgO)<sub>0.9</sub> at the same wavelength equal  $7.68 \times 10^{-6}$ , and for Coal samples the extinction coefficient value at 272 nm equal for the Coal<sub>0.5</sub>(MgO)<sub>0.1</sub> sample equal  $1.5 \times 10^{-6}$ , but for Coal<sub>0.5</sub>(MgO)<sub>0.9</sub> sample equal  $6.71 \times 10^{-6}$  at the same wavelength. The effects of Magnesium Oxide (MgO) doping on (Soot and Coal) samples doping by rate (0.1, 0.3, 0.5, 0.7 and 0.9) was increased the Magnesium Oxide (MgO) doping decreased Extinction coefficient (k). The optical energy gap ( $E_g$ ) has been

calculated by the relation  $(\alpha h\nu)^2 = C(h\nu - E_g)$  where (C) is constant. By plotting  $(\alpha h\nu)^2$  vs photon energy (hν) as shown in fig.(4.19 ) for the (Soot and Coal) doping by Magnesium Oxide (MgO) (0.1, 0.3, 0.5, 0.7 and 0.9) ratio samples. By extrapolating the straight thin portion of the curve to intercept the energy axis, the value of the energy gap has been calculated. In fig (4.19) the value of ( $E_g$ ) Soot samples that was not doping by magnesium oxide sample Soot<sub>0.5</sub>( MgO)<sub>0.0</sub> obtained was (3.517) eV but for Soot<sub>0.5</sub>( MgO)<sub>0.1</sub> equal ( 3.513) eV , and when reach sample Soot<sub>0.5</sub>( MgO)<sub>0.9</sub> equal ( 3.499) eV. The value of( $E_g$ ) was decreased from (3.517) eV to (3.499) eV. For the coal samples that was not doping by magnesium oxide sample Coal<sub>0.5</sub>( MgO)<sub>0.0</sub> obtained was (3.502) eV but for Coal<sub>0.5</sub> ( MgO)<sub>0.1</sub> equal ( 3.487) eV , and when reach sample Coal<sub>0.5</sub>( MgO)<sub>0.9</sub> equal ( 3.398) eV . The value of( $E_g$ ) was decreased from (3.502) eV to (3.398) eV. The decreasing of ( $E_g$ ) related to increase of magnesium oxide molar on the samples. It was observed that the different Magnesium Oxide (MgO) ratio for Soot and Coal) doping by Magnesium Oxide (MgO) (0.1, 0.3, 0.5, 0.7 and 0.9) ratio samples confirmed the reason for the band gap shifts.

#### **4.4.1 I-V characteristics multilayers diode Results of Carbon Nano Tube (CNT) doping by (MgO)**

After made Carbon Nano Tube (CNT) from (Soot and Coal) and doping by Magnesium Oxide (MgO) in different ratio (0.1, 0.3, 0.5, 0.7 and 0.9). Then fabrication of the device was through spin casting of Carbon Nano Tube (CNT) from (Soot and Coal) and doping by Magnesium Oxide (MgO) in different ratio and MEH-PPV and this category of device exhibits current and voltage turn on.

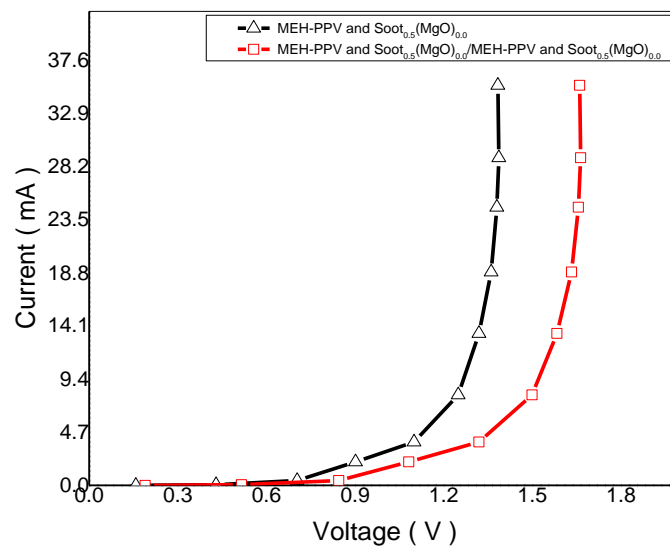


Fig (4.20) I-V characteristics of Soot Carbon Nano Tube (CNT) doping by Magnesium Oxide (MgO) <sub>0.0</sub>

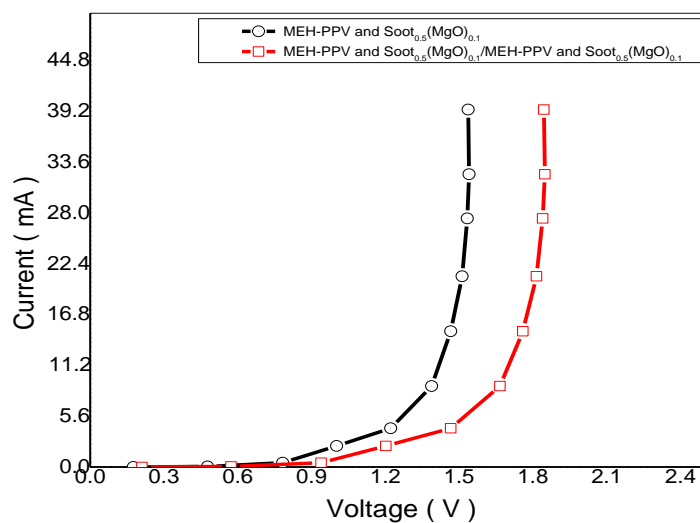


Fig (4.21) I-V characteristics of Soot Carbon Nano Tube (CNT) doping by Magnesium Oxide (MgO) <sub>0.1</sub>

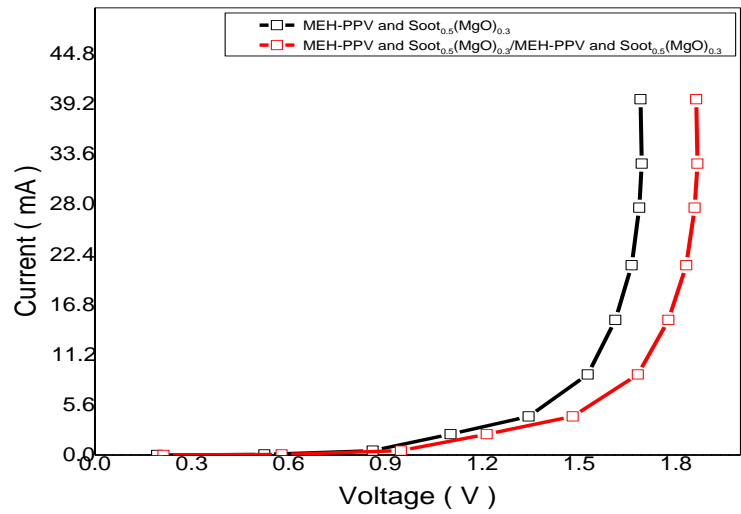


Fig (4.22) I-V characteristics of Soot Carbon Nano Tube (CNT) doping by Magnesium Oxide (MgO) <sub>0.3</sub>

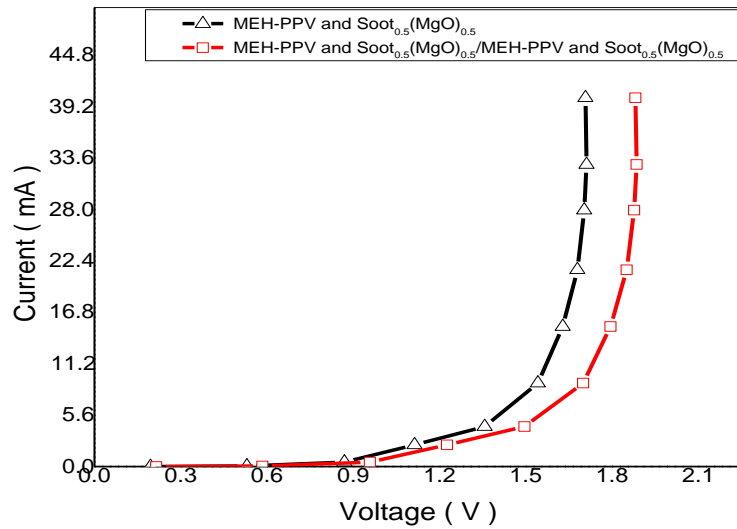


Fig (4.23) I-V characteristics of Soot Carbon Nano Tube (CNT) doping by Magnesium Oxide (MgO) <sub>0.5</sub>

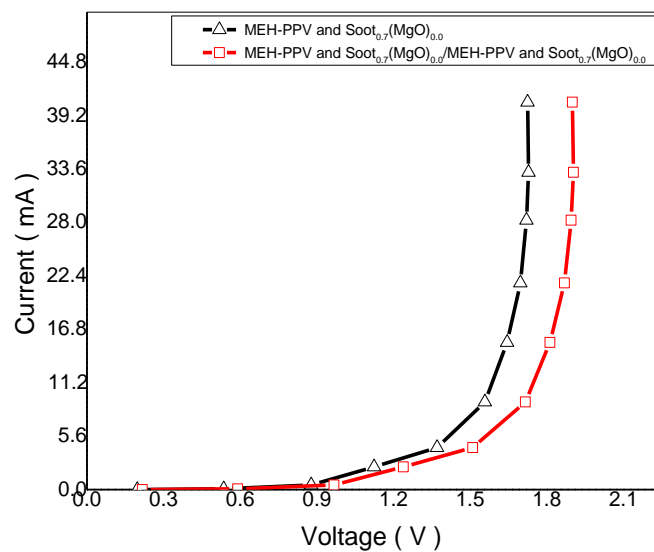


Fig (4.24) I-V characteristics of Soot Carbon Nano Tube (CNT) doping by Magnesium Oxide (MgO) <sub>0.7</sub>

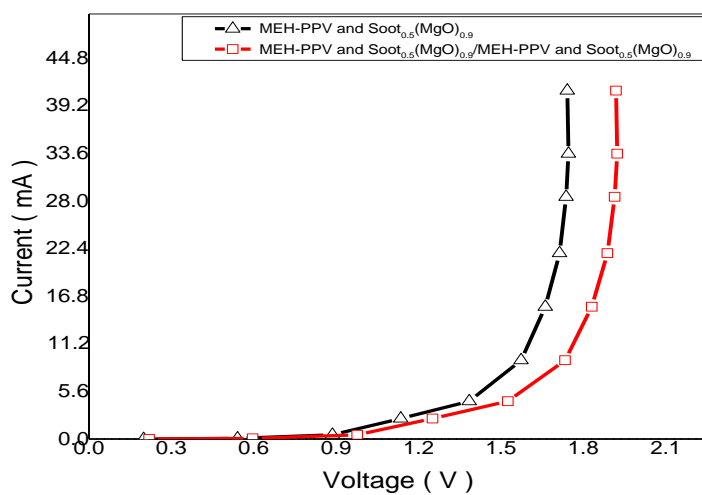


Fig (4.25) I-V characteristics of Soot Carbon Nano Tube (CNT) doping by Magnesium Oxide (MgO) <sub>0.9</sub>

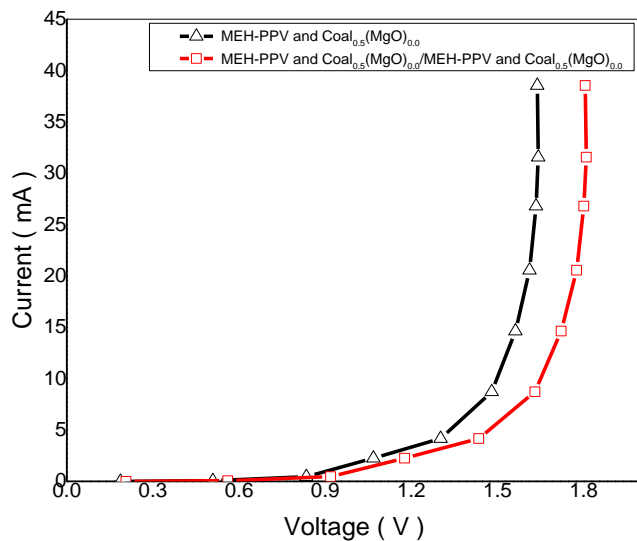


Fig (4.26) I-V characteristics of Coal Carbon Nano Tube (CNT) doping by Magnesium Oxide (Mg O)<sub>0.0</sub>

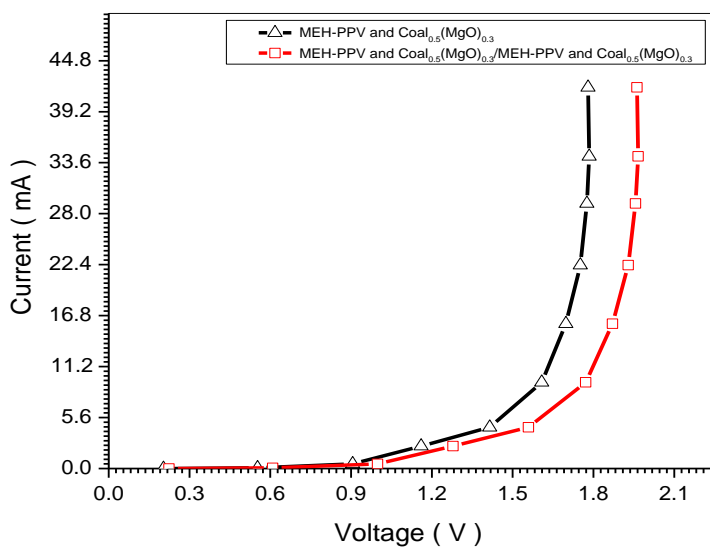


Fig (4.27) I-V characteristics of Coal Carbon Nano Tube (CNT) doping by

### Magnesium Oxide (MgO)<sub>0.1</sub>

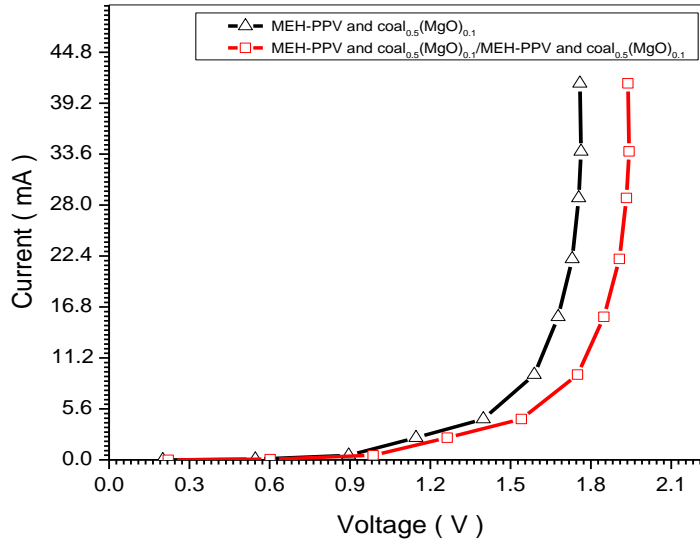


Fig (4.28) I-V characteristics of Coal Carbon Nano Tube (CNT) doping by Magnesium Oxide (MgO)<sub>0.3</sub>

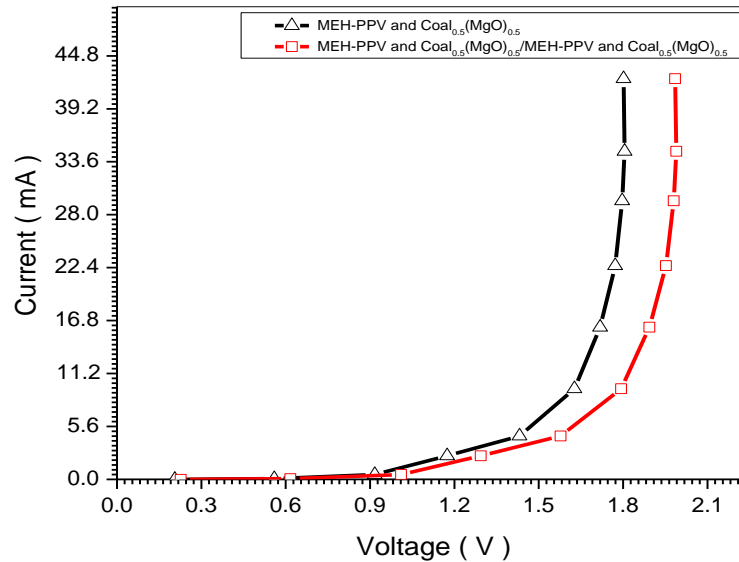


Fig (4.29) I-V characteristics of Coal Carbon Nano Tube (CNT) doping by Magnesium Oxide (MgO)<sub>0.5</sub>

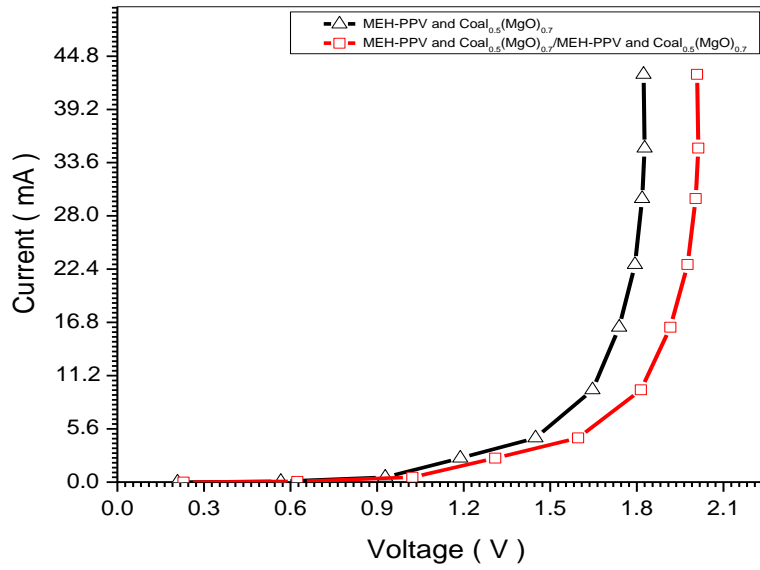


Fig (4.30) I-V characteristics of Coal Carbon Nano Tube (CNT) doping by Magnesium Oxide (MgO)  $0.7$

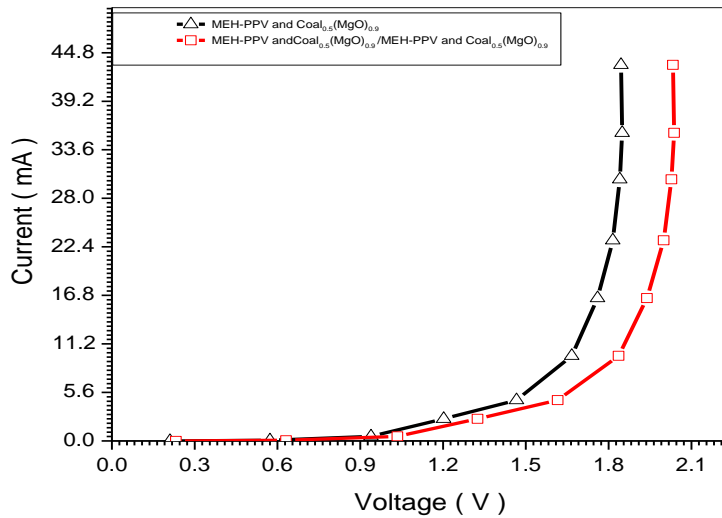


Fig (4.31) I-V characteristics of Coal Carbon Nano Tube (CNT) doping by Magnesium Oxide (MgO)  $0.9$

Table (4.5) threshold of charge injection and highly twistable device had shown a turn on voltage of Carbon Nano Tube (CNT) from (Soot and Coal) and doping by Magnesium Oxide (Mg O) in different molar (0.1, 0.3, 0.5, 0.7 and 0.9)

No	Samples	charge injection voltage ( V )		turn on voltage ( V )	
		single layer	double layers	single layer	double layers
1	Coal <sub>0.5</sub> (MgO) <sub>0.0</sub>	1.38323	1.65988	0.15786	0.18943
2	Coal <sub>0.5</sub> (MgO) <sub>0.1</sub>	1.53692	1.84431	0.1754	0.21048
3	Coal <sub>0.5</sub> (MgO) <sub>0.3</sub>	1.69062	1.86275	0.19294	0.21258
4	Coal <sub>0.5</sub> (MgO) <sub>0.5</sub>	1.70752	1.88138	0.19487	0.21471
5	Coal <sub>0.5</sub> (MgO) <sub>0.7</sub>	1.7246	1.90019	0.19681	0.21685
6	Coal <sub>0.5</sub> (MgO) <sub>0.9</sub>	1.74184	1.91919	0.19878	0.21902
7	Soot <sub>0.5</sub> (MgO) <sub>0.0</sub>	1.63837	1.80518	0.18697	0.20601
8	Soot <sub>0.5</sub> (MgO) <sub>0.1</sub>	1.75909	1.9382	0.20075	0.22119
9	Soot <sub>0.5</sub> (MgO) <sub>0.3</sub>	1.7802	1.96145	0.20316	0.22384
10	Soot <sub>0.5</sub> (MgO) <sub>0.5</sub>	1.80156	1.98499	0.2056	0.22653
11	Soot <sub>0.5</sub> (MgO) <sub>0.7</sub>	1.82318	2.00881	0.20806	0.22925
12	Soot <sub>0.5</sub> (MgO) <sub>0.9</sub>	1.84506	2.03292	0.21056	0.232

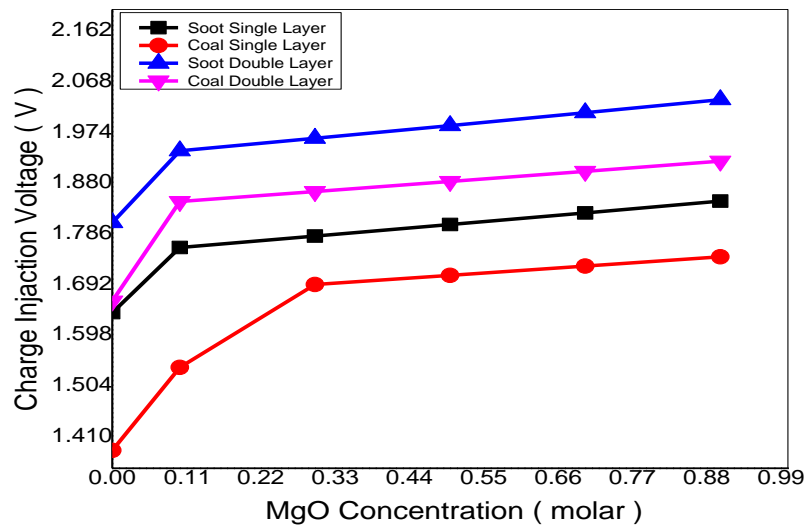


Fig (4.32) relationship between concentration of Magnesium Oxide (MgO) and charge injection voltage for Carbon Nano Tube (CNT) from (Soot and Coal)

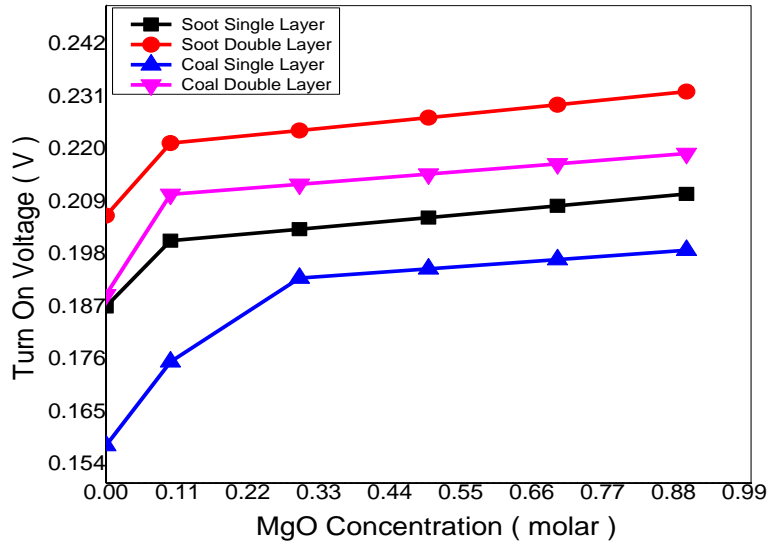


Fig (4.33) relationship between concentration of Magnesium Oxide (MgO) and turn on Voltage for Carbon Nano Tube (CNT) from (Soot and Coal)

#### 4.4.2 I-V characteristics multilayers Discussion of Carbon Nano Tube (CNT) doping by (MgO)

The I-V characteristics of Carbon Nano Tube (CNT) from soot and doping by Magnesium Oxide (MgO) 0.0 ratio shows from fig (4.20) to fig (4.25) related to diode, a threshold of charge injection of around 1.63837V for single layer (MEH-PPV – soot (MgO) 0.0) and 1.8051814 V for double layers (MEH-PPV – soot (MgO) 0.0 / MEH-PPV – soot (MgO) 0.0), 1.75909 V for single layer (MEH-PPV – soot (MgO) 0.1) and 1.9382 V for double layers (MEH-PPV – soot (MgO) 0.1 / MEH-PPV – soot (MgO) 0.1), 1.7802 7V for single layer (MEH-PPV – soot (MgO) 0.3) and 1.96145 V for double layers (MEH-PPV – soot (MgO) 0.3 / MEH-PPV – soot (MgO) 0.3), 1.80156 V for single layer (MEH-PPV – soot (MgO) 0.5) and 1.98499 V for double layers (MEH-PPV – soot (MgO) 0.5 / MEH-PPV – soot (MgO) 0.5), 1.82318 V for single layer (MEH-PPV – soot MgO) 0.7) and 2.00881

V for double layers (MEH-PPV – soot (MgO) 0.7 / MEH-PPV – soot (MgO) 0.7) and 1.84506 V for single layer (MEH-PPV – soot (MgO) 0.9) and 2.03292 V for double layers (MEH-PPV – soot (MgO) 0.9 / MEH-PPV – soot (MgO) 0.9), and a high turn on voltage making very high power consumption. Later, flexible soot Carbon Nano Tube (CNT) doping by (MgO) by spin coating a layer of poly aniline onto a sheet of poly ethylene terephthalate, Poly (2-methoxy, 5-(2-ethylhexoxy)-1, 4- phenylene -vinylene (MEH- PPV) used ITO glass as cathode. The robust and highly twistable device had shown a turn on voltage at 0.18697 V for single layer (MEH-PPV – soot (MgO) 0.0) and 0.20601 V for double layers (MEH-PPV – soot (MgO) 0.0 / MEH-PPV – soot (MgO) 0.0) , at 0.20075 V for single layer (MEH-PPV – soot (MgO) 0.1) and 0.22119 V for double layers (MEH-PPV – soot (MgO) 0.1 / MEH-PPV – soot (MgO) 0.1) at 0.20316 V for single layer (MEH-PPV – soot (MgO) 0.3) and 0.22384 V for double layers (MEH-PPV – soot (MgO) 0.3 / MEH-PPV – soot (MgO) 0.3) , at 0.2056 V for single layer (MEH-PPV – soot (MgO) 0.5) and 0.22653 V for double layers (MEH-PPV – soot (MgO) 0.5 / MEH-PPV – soot (MgO) 0.5) , at 0.20806 V for single layer (MEH-PPV – soot (MgO) 0.7) and 0.22925 V for double layers (MEH-PPV – soot (MgO) 0.7 / MEH-PPV – soot (MgO) 0.7) and at 0.21056 V for single layer (MEH-PPV – soot (MgO) 0.9) and 0.232 V for double layers (MEH-PPV – soot (MgO) 0.9 / MEH-PPV – soot (MgO) 0.9) as shown from Fig (4.20) to fig (4.25) .

The I-V characteristics of Carbon Nano Tube (CNT) from cool and doping by Magnesium Oxide (MgO) 0.0 ratio shows from fig (4.26) to fig (4.31) a threshold of charge injection of around 1.383237V for single layer (MEH-PPV – cool (MgO) 0.0) and 1.65988 V for double layers (MEH-PPV – cool (MgO) 0.0 / MEH-PPV – cool (MgO) 0.0) , 1.53692 V for single layer (MEH-PPV – cool (MgO) 0.1) and 1.84431 V for double layers (MEH-PPV – cool (MgO) 0.1 / MEH-PPV – cool (MgO) 0.1), 1.69062 V for single layer (MEH-PPV –Coal (MgO) 0.3) and 1.86275

V for double layers (MEH-PPV – cool(MgO) 0.3 / MEH-PPV – cool (MgO) 0.3), 1.70752 V for single layer (MEH-PPV – cool (MgO) 0.5) and 1.88138V for double layers (MEH-PPV – cool (MgO) 0.5 / MEH-PPV – cool (MgO) 0.5) , 1.7246 V for single layer (MEH-PPV – cool (MgO) 0.7) and 1.90019 V for double layers (MEH-PPV – cool (MgO) 0.7 / MEH-PPV – cool (MgO) 0.7) and 1.74184 V for single layer (MEH-PPV – cool (MgO) 0.9) and 1.91919 V for double layers (MEH-PPV – cool (MgO) 0.9 / MEH-PPV – cool (MgO) 0.9), and a high turn on voltage making very high power consumption. Later, flexible cool Carbon Nano Tube (CNT) doping by (MgO) by spin coating layer of poly aniline onto a sheet of poly ethylene terephthalate, Poly (2-methoxy, 5-(2-ethylhexoxy)-1, 4- phenylene - vinylene (MEH- PPV) used ITO glass as cathode . The robust and highly twistable device had shown a turn on voltage at 0.15786 V for single layer (MEH-PPV – cool (MgO) 0.0) and 0.18943 V for double layers (MEH-PPV – cool (MgO) 0.0 / MEH-PPV – cool (MgO) 0.0) , at 0.1754 V for single layer (MEH-PPV – cool (MgO) 0.1) and 0.21048 V for double layers (MEH-PPV – cool (MgO) 0.1 / MEH-PPV – cool (MgO) 0.1) at 0.19294 V for single layer (MEH-PPV – cool(MgO) 0.3) and 0.21258 V for double layers (MEH-PPV – cool (MgO) 0.3 / MEH-PPV – cool (MgO) 0.3) , at 0.19487 V for single layer (MEH-PPV – cool (MgO) 0.5) and 0.2147 V for double layers (MEH-PPV – cool (MgO) 0.5 / MEH-PPV – cool (MgO) 0.5) , at 0.19681 V for single layer (MEH-PPV – cool (MgO) 0.7) and 0.21685 V for double layers (MEH-PPV – cool (MgO) 0.7 / MEH-PPV – cool (MgO) 0.7) and at 0.19878 V for single layer (MEH-PPV – cool (MgO) 0.9) and 0.21902 V for double layers (MEH-PPV – cool (MgO) 0.9 / MEH-PPV – cool (MgO) 0.9) as shown from Fig (4.26) to fig (4.31).

All this results keeping in table (4.5). In Fig (4.32) and Fig (4.33) show the relationship between the concentration of MgO that doping for the (Soot, Coal) Carbon Nano Tube (CNT) samples and (Charge Injection Voltage and Turn On

Voltage), it's clear that the Charge Injection Voltage and Turn On Voltage increases with concentration increases, also the value of Charge Injection Voltage and Turn On Voltage for the soot (single and double) greater than the coal (single and double) due to energy band gap and crystal structure .

#### **4.5 General Discussion**

According to XRD analysis we found the change in source of carbon nanotube and concentration of MgO, change the structure of CNT, it was observed the grain size of CNT increases when the concentration of MgO increases for both source of CNT, the grain size of CNT from coal greater than the grain size from soot since soot is one of coal composite. It was also observed that. The distance between planes of CNT from soot was decreased when concentration of MgO increases while it was increases when concentration of MgO increases for CNT from coal, and this is refer to porous natural. The crystal type change due to source of CNT and concentration change. The density decrease when the concentration increases for both source, as general the density of CNT prepared from soot greater than the density of CNT prepared from coal, according for this reason the absorbance and optical energy band gap were decreased, the absorbance of CNTs from soot greater than the absorbance of CNTs from coal, the optical band gap for both source of CNTS within range of semiconductor materials (3.392-3.517) eV. FTIR result show that the all sample of CNT ( soot – coal) interact with IR spectrum as same way, the transmittance of IR through CNT prepared from (soot-coal) increases when the concentration of MgO increased this confirm with the fact of lightness of soot and porous in coal . It was noted the change in concentration did not change the vibrational frequencies of the samples of CNTS from soot and coal. All samples of CNTS from soot and coal had same functional group, it was observed that CNTs from coal more stable than CNTs from soot and this refer to that all

most of bond in CNTs from coal were single bond rather than CNTs from soot . I - V curve display that samples acts as diode multilayer, the charge injection voltage and turn off voltage increases when the concentration of MgO and number of layer increases for CNTS made from soot and coal which lead to increase the number of free electrons and these confirm with the previous studies.

#### **4.6 conclusion**

Carbon nanotube doping by MgO were preparing using thermal chemical method. The change in source of CNTS and concentration of MgO lead to change the structural parameters of CNTS, which means change the optical properties, due to optical energy band gap, the CNTs from coal best than CNTs from soot as semiconductor material. Diode multilayers were fabricated from CNTS prepared from two source and doping by MgO at different molar, the charge injection voltage and turn on voltage increases the concentration of MgO and number of layer increases.

#### **4.7 Recommendations**

- To syntheses CNTs using anther method.
- Study additional properties of carbon nanotubes (mechanical, thermal and magnetic)
- To syntheses and study properties of MCNTs doping by MgO.

## Referance

- Abazari, S., Shamsipur, A., Reza, H., Fauzi, A., Sharif, S., Razzaghi, M., Ramakrishna, S. and Filippo M.(2020).Carbon Nanotubes (CNTs)-Reinforced Magnesium-Based Matrix Composites: A Comprehensive Review
- AbdulBaki, M., Tangonan, A., Advincula, R., Randall , T. and Krishnamoorti , R.( 2011). Properties of Single-Walled Carbon Nanotube-Based Poly(phenylene vinylene) Electroluminescent Nano composites , DOI: 10.1002/polb.23007.
- Ahmad, I., Cao, H., Chen, H., Kennedy, A., Zhao, H., Zhu, Y .(2016).CARBON NANOTUBES-REINFORCING MgO-DOPED Al<sub>2</sub>O<sub>3</sub> NANOCOMPOSITES.
- Ali, M., Das, R., Maamor, A. and Hamid, S. (2014).Multifunctional carbon nanotubes (CNTs): a new dimension in environmental remediation. Adv Mat Res 832:328–32.
- Aloui, w ., Hamza, s., and Bouazizi , a.(2016).Comparative Study of Deposit through a Membrane and Spin-Coated MWCNT as a Flexible Anode for Optoelectronic Applications.
- Anvari, A. (2017) . Effect of nano-carbon percentage on properties of composite materials.
- Batani, D., Vinci, T. and Bleiner, D. (2014). Laser-ablation and induced .
- Becker, M.F., Brock, J.R., Cai, H., Chaudhary, N., Henneke, D. and Hilsz, L., Keto, J.W.,- Lee, J., Nichols, W.T., Glicksman, H.D. (1997) . Nanoparticles generated by laser ablation. In Proc. Of the Joint NSF-NIST Conf. on Nanoparticles.
- Bunaciu, A.A., UdriTioiu, E.G. and Aboul-Enein, H.Y. (2015). X-ray diffraction.
- Chand, E., Campbe, P., Baumann, T. and Worsley, M.(2017). Carbon aerogel evolution, Allotrope, Grapheme-inspired, and 3D-printed aerogels.
- Charlier, A., McRae, E., Heyd, R., Charlier, M.F. and Moretti, D.(1999).Carbon Classification for double-walled carbon nanotubes .
- Chehata, N., Dhibi, O., Ltaief, A., Farzi, A. and Bouazizi, A.( 2012).Charge Transfer Properties in MEH-PPV/PS:MWCNTs Nanocomposites.
- Chen, C. C., Aykol, M., Chang, C. C., Levi, A. F. J. and Cronin, S. B. (2011) . Graphene-silicon Schottky diodes. Nano Lett. 11.
- Chen, C., Liao, C., Wei, L., Zhong, H., He, R., Liu, X., Lai, Y., Song, C., Jin, T. and Zhang, Y .(2016).Carbon nanotube intramolecular p-i-n junction diodes with symmetric and asymmetric contacts

Chen, J. (2005). "Bright Infrared Emission from Electrically Induced Excitons in Carbon Nanotubes". *Science*. 310 (5751).

Chen, P., Wu, X., Sun, X., Lin, J., Ji, W. and Tan, K. L. (1999). Electronic structure and optical limiting behavior of carbon nanotubes . *Physical Review Letters*.

Comfort , E. and Ung , J .(2016).Large Bandgap Shrinkage from Doping and Dielectric Interface in Semiconducting Carbon Nanotubes , number: 28520 .

Dai, H. (2001).Carbon nanotubes: opportunities and challenges,quantification and environmental recalcitrance.

Das, R., Shahnavaz, Z., Eaqub, M., Moinul, M. and Abd Hamid, S. (2016).Can We Optimize Arc Discharge and Laser Ablation for Well-Controlled Carbon Journet.

Master, W.K., Berneir, P. and Loisequ, A. (1997). Large scale production of single wall carbon nano tubes by electric arc technique” *Nature* volume ,Nanotube Synthesis .

Dasa, R., Abd Hamida, S., Alia, M., Ramakrishnab, S.and Yongzhi, W. (2015). Carbon Nanotubes Characterization by X-ray Powder Diffraction – A Review .

Delhaes, P. (2000).Graphite and precursors .

den , J.V., Langergraberb, G. and Weingartne , A. (2006).On-line and in-situ UV/vis

DEWIT, J. and SEAGER , S. (2013) . Constraining Exoplanet Mass from Transmission Spectroscopy , DOI: 10.1126/science.1245450 .

Dobrzańska-Danikiewicz, A.D., Łukowiec, D., Cichocki, D. and Wolany, W. (2013). Carbon nanotubes decorating methods

Donald, L., Gary , M., ‘ George , S., James , A . (2015 ).Introduction to Spectroscopy . WCN: 20-2000-2008.

Dresselhaus, G., Dresselhaus, M. and Saito, R. (1998 ).Physical properties of carbon nanotubes.

E.N. Ganesh. (2013).Single Walled and Multi Walled Carbon Nanotube Structure, Synthesis and Applications.

Ebbesen, T.W. and Ajayan, P.M. (1992).“Large-scale synthesis of carbon nanotubes,” *Nature*.

Freitag, M. (2003)."Photoconductivity of Single Carbon Nanotubes ,*nano Letters*. 3 (8). doi:10.1021/nl034313e.

Gadipelli, S., Li, Z., Zhao, T., Yang, Y., Yildirim, T. and Guo, Z. (2017).Graphitic nanostructures in a porous carbon framework significantly enhance electrocatalytic oxygen evolution.

Ganesh, E.N. (2013).Single Walled and Multi Walled Carbon Nanotube Structure, Synthesis and Applications .

Gattia, D.M., Antisan, M.V., Marazzi, R., Pilloni, L. and Contini, V., Montone, A. (2006).Arc-discharge synthesis of carbon nano horns and multi walled carbon nanotubes.

Georgakilas, V., Perman, J.A., Tucek, J., Zboril, R. (2015). Broad Family of Carbon Nanoallotropes: Classification, Chemistry, and Applications of Fullerenes, Carbon Dots, Nanotubes, Graphene, Nanodiamonds, and Combined Superstructures.

Gouda1, P.S., Kulkarni, R., Kurbet, S.N. and Jawali, D. (2013). Effects of Multi Walled Carbon Nanotubes and Graphene on the Mechanical Properties.

Gupta, A., Pandey, A. and Shrivastava , A. K. ( 2017).Role of Zener Diode and Its Application.

Habeb, F., Fadel, A. and Hasan, F. (2019).Behavior of X-Ray Analysis of Carbon Nanotubes .

Hameed, tm., Aneesh, A., Baiju, M. and Predeep, P. (2011).Comparison of electricaland optical behaviors of MEH-PPV andMEH-PPV/CNT blend based polymer light emitting diodes.

Hammond , H., (2015).The Basics of Crystallography and Diffraction.

Harris, B., Bunsell, A.R. (1977).Structure and Properties of Engineering Materials, Longman, London, New York .

Hatton, A. Miller, J. and Silva, S.R.P. (2008).Carbon nanotubes: a multi-functional material for organic optoelectronics .

Haur, C., Lung, C., Ming, W., Tzu, Y., Cheng, C., Shan, Y., Hao, C., Yu, C. and Chen, H . (2017 ).Magnesium Oxide (MgO) pH-sensitive Sensing Membrane in Electrolyte-Insulator-Semiconductor Structures with CF4 Plasma Treatment.

Heavens , O. S. (1991).Optical Properties of Thin Solid Films . QC 176.84.07H43.

Hokkanen, M.J., Lautala, S., Shao, D., Turpeinen, T., Koivistoinen, J. and Ahlskog, M. (2016).On-chip purification via liquid immersion of arc-discharge synthesized multiwalled carbon nanotubes. Appl Phys A 122(7):1-8. nanoparticle synthesis. Laser Part Beams ,32(1).

Hone, J., Batlogg, B., Benes, Z., Johnson, A. and Fischer, J. (2000).Quantized phonon spectrum of single-wall carbon nanotubes. Science 289(5485):1730.

Hussein, A., AL-Hassani, E. and Subhi, M. (2017).Mechanical and Physical Properties of Nano Carbon Tube with Carbon Fiber Reinforced with Polyester Resin.

Hyung, J., Min, C., Hyun, J., Hyuk, J., Hyun, J., Joo, J., Hee, Y., Nam, W. and Joong, C. (2009).Doping Effect of CNT and Nano-Carbon inMagnesium Diboride Bulk .

Iijima, S., Ichihashi, T., Nature, D.S., Bethune, C.H., Kiang, M.S., Devries, G., Gorman, R. and Savoy, J., Vazquez, A. (1993). Nature;4.

Iijima, S. (1991). Helical microtubules of graphitic carbon.

Iijima, S. and Ichihashi, T. (1992). Single cell carbon nano tube of nanometer diameter” Nature.

Ikram, M., Inayat, T., Haider, A., Ul-Hamid, A., Haider, J., Nabgan, W., Saeed, A., Shahbaz, A., Hayat, S., Ul-Ain, K. and Butt, A. (2021). Graphene Oxide-Doped MgO Nanostructures for Highly Efficient Dye Degradation and Bactericidal Action Instrumentation and applications. Critical Reviews in Analytical Chemistry, 45(4).

Johannsen, I., Jaksik, K., Wirch, N., Pötschke, P., Fiedler, B. and Schulte, K. (2016) . Electrical conductivity of melt-spun thermoplastic poly (hydroxy ether of bisphenol) fibres containing multi-wall carbon nanotubes. Polymer, 97,8094 .

Johannsen, I., Jaksik, K., Wirch, N., Pötschke, P., Fiedler, B. and Schulte, K. (2016). Electrical conductivity of melt-spun thermoplastic poly (hydroxy ether of bisphenol) fibres containing multi-wall carbon nanotubes. Polymer 97.

Journet, C., W. K. Maser, W.K., Bernier, P. (1997). “Large-scale production of single-walled carbon nanotubes by the electric-arc technique.

Ka, I., LeBorgne, V., Fujisawa, K., Hayashi, T., Kim, Y.A. and Endo, M. (2016) . Multiple exciton generation induced enhancement of the photoresponse of pulsed-laser-ablation synthesized single-wall-carbon-nanotube/PbS-quantum-dots nanohybrids.

Kaviyarasu, K. and Anand, P. (2011). Synthesis and characterization studies of cadmium doped MgO nanocrystals for optoelectronics application .

Kharisov, B.I., Kharissova, O.V. (2019 ). Carbon Allotropes, Metal-Complex Chemistry, Properties and Applications.

Kim, P., Odom, T., Huang, J. and Lieber, C. (2000) . Carbon, 38.

kim, sm., Gangloffab, I. (2011). Thermal chemical vapor deposition (T-CVD) growth of carbon nanotubes on different metallic underlayers .

Kong, J., Cassell, A.M. and Dai, H. (1998). Chemical vapor deposition of methane for single-walled carbon nanotubes,” Chemical Physics Letters.

Krueger, A. (2010 ). Carbon materials and nanotechnology.

Kuhlbusch, T.A.J., Crutzen, P.J. (1996). Black carbon, the global carbon cycle, and atmospheric carbon dioxide.

Lee, R.S., Kim, H.J., Fischer, J.E. and Thess, A., Smalley, R.E. (1997) . Conductivity enhancement in single-walled carbon nanotube bundles doped with K and Br

LI, B., Migan, A., Delpha, C., Dilallo, D. (2020). Analysis of the Performance of I-V Curve Correction Methods in the Presence of Defects.

Li, L. and Han, M. (2015). A Novel Way for Determining Bravais Lattice Using a Single Electron Backscatter Diffraction Pattern

Lischke, S., Kno, D., Mai, C., Zimmermann, L., Peczek, A., Kroh, M., Trusch, A., Krone, E., Voigt, K. and Ma, A. (2015). High bandwidth, high responsivity waveguide-coupled germanium p-i-n photodiode

Liu, S., Xiu, H., Zhang, H. (2014). Tunable ultrathin mantle cloak via varactor-diode-loaded metasurface.

M. Su, B. Zheng, and J. Liu. (2000). "A scalable CVD method for the synthesis of single-walled carbon nanotubes with high catalyst productivity," *Chemical Physics Letters*, vol. 322, no. 5.

Ma, P.C., Tang, B.Z. and Kim, J.K. (2008). Effect of CNT decoration with silver nanoparticles on electrical conductivity of CNT/polymer composites," *Carbon*, 11.

Marais, B., Brittle, W., Painczyk, K., Anneke, C., Beyers, N., Wasserman, E., Soelingen, D., DWarren, R. (2008). Use of Light-Emitting Diode Fluorescence Microscopy to Detect Acid-Fast

Matsu, N. (2018). Synthesis of Acetylenic Carbon Molecules via Pulsed Laser Ablation in Ethanol.

Miles, J., Wien, F., Wallace, B.A. (2004). Redetermination of the extinction coefficient of camphor-10-sulfonic acid, a calibration standard for circular dichroism spectroscopy.

Mirabile, D., Vittori, M., Marazzi, R., Pilloni, L., Contini, V. and Montone, A. (2006). Arc-discharge synthesis of carbon nano horns and multi walled carbon nanotubes, 518.

Mirzaei, H., Davoodnia, A. (2012). Microwave assisted sol-gel synthesis of MgO nanoparticles and their catalytic activity in the synthesis of hantzsch 1, 4-dihydropyridines. *Chin J Catal* 33.

Misewich, J. (2003). Electrically Induced Optical Emission from a Carbon Nanotube FET". *Science*. 300 (5620).

Moeck, P., DeStefano, P. (2018). Accurate lattice parameters from 2D-periodic images for subsequent Bravais lattice type assignments.

Morimoto, Y., Horie, M., Kobayashi, N., Shinohara, N. and Shimada, M. (2013). Inhalation toxicity assessment of carbon-based nanoparticles. *Acc Chem Res*; 46.

Nemeth, K., Varro, N., Reti, P., Berki, P., dam, B., Belina, K. and Hernadi, K. (2019). Synthesis and investigation of SiO<sub>2</sub>-MgO coated MWCNTs and their potential application agents.

Poonguzhali, R., Gobi, R., Shanmuga, M. and Karthik, v. (2017). Synthesis and Characterization of Ce Doped MgO Nanocrystals .

Ravishankar, R.V., Jamuna, B.A. (2011). Nanoparticles and their potential application as antimicrobials. *Science against microbial pathogens. Communicating current research and technological advances.* A. Me´ndez-Vilas (Ed.), pp 197–209.

safa .(2001). PN junction devices and light emission diode .

Seeger , K. ( 2013). *Semiconductor Physics* , 73- 104 13.

Semple, J., Georgiadou, D. G., Wyatt, G ., Gelinck, G. , Anthopoulos, T. D. and Techno, S. (2009). *Semicond* 206, 588.

Shalini, C. and Pragnesh, N.D. (2012). *Microscopy in Nanotechnology.* Department of Chemistry; Kachchh University; Kachchh- 370001, Gujarat India.

Shenderova, OA., Gruen, DM. (2012). *Ultrananocrystalline diamond: synthesis, properties and applications.*

Shi, S., and Ravi , S.( 2014). *High Luminance Organic Light-Emitting Diodes with Efficient Multi-Walled Carbon Nanotube Hole Injectors .*

Singh, E., Srivastava, R., Utkarsh Kumar, U. and Katheria, A. (2017). *Carbon Nanotube: A Review on Introduction, Fabrication Techniques and Optical Applications*, 4(4).

Slavík , J . (1989). *Intracellular pH and its Measurement Spectroscopy for multi-parameter measurements: a brief review* VOL. 18 NO. 4.

Sufri, M ., Kamarulzaman, N., Azizi, M ., Maria, A., Rusdi, R . and Kamarudin, N .(2014). *Growth mechanisms of MgO nanocrystals via a sol-gel synthesis using different complexing*

Tandabany, C., Dinadayalane , D., Leszczynski, J. (2009). *Fundamental Structural, Electronic, and Chemical Properties of Carbon Nanostructures: Graphene, Fullerenes, Carbon Nanotubes, and Their Derivatives.*

Thess, A., Lee, R., Nikolaev, P. (1996). “Crystalline ropes of metallic carbon nanotubes,” *Science*, 5274, pp. 483–487.

Tiwari, A. (2016). Benchmark study of Carbon Nanotubes and Synthesis of Single Wall Nanotube by Thermal Chemical Vapor Deposition (TCVD) Method.

Vaijayanthimala, V., Chang, H.C. (2009). Functionalized fluorescent nanodiamonds for biomedical applications .

Varshney, K. (2014). Carbon nanotubes: A review on synthesis, properties and applications, *Int J Eng Res Gen Sci.* 2(4).

WanderWal, R.L., Berger, T.M. (2003). Carbon nano tube synthesis in aflame using laser ablation for insitu catalyst generation” *Applied Physics* .

Wang , S., Wang , Y., Ramasse, Q. and Fan , Z. (2020 ) . The Nature of Native MgO in Mg and Its Alloys , 51.

Wong, E., Sheehan, P. and Lieber, C. (1997). Nano beam mechanics: elasticity, strength, and toughness of nanorods and nanotubes. *Science* 277(5334):1971–5.

Yaceman, M., Yoshida, M., Rendson, J and Santiestaban, G. (1993). “ Catalytic growth of carbon micro tubules with fullerene structure” *Applied physics letter* volume – 62.

Yi, z ., Sayago, j. (2019). Incorporating aligned carbon nanotube electrode arrays in organic thin-film transistors , 045025.

Yosef, Z., YACOB , James, J., Monika , T. and Michelle , M. (2003). Absorption spectroscopy of colored dissolved organic carbon in Georgia (USA) rivers: the impact of molecular size distribution.

Yusof, Y., Irwan, M., Rafie, M .(2016). Enhanced Structural, Thermal, and Electrical Properties of Multiwalled Carbon Nanotubes Hybridized with Silver Nanoparticles.

ZH, X., Guduru, P.R. and Curtin, W.A. (2007 ). Enhancing mechanical properties of multiwall carbon nanotubes via  $sp^3$  interwall bridging, *Physical Review Letters* ; 98.

Zheng, X., Li, J. and Zhou, Y . (2004). X-ray diffraction measurement of residual stress in PZT thinfilms prepared by pulsed laser deposition.

Zondlo, J.W. (2012). Graphite, structure, properties, and applications.